CARDIOVASCULAR DISEASE

Structure-Guided Design of a High-Affinity Platelet Integrin $\alpha_{IIb}\beta_3$ Receptor Antagonist That Disrupts Mg^{2+} Binding to the MIDAS

Jieqing Zhu,[1,2]* Won-Seok Choi,[3]* Joshua G. McCoy,[4]* Ana Negri,[5]* Jianghai Zhu,[1]* Sarasija Naini,[3] Jihong Li,[3] Min Shen,[4] Wenwei Huang,[4] Daniel Bougie,[2] Mark Rasmussen,[2] Richard Aster,[2] Craig J. Thomas,[4] Marta Filizola,[5] Timothy A. Springer,[1] Barry S. Coller[3]†

An integrin found on platelets, $\alpha_{IIb}\beta_3$ mediates platelet aggregation, and $\alpha_{IIb}\beta_3$ antagonists are effective antithrombotic agents in the clinic. Ligands bind to integrins in part by coordinating a magnesium ion (Mg^{2+}) located in the β subunit metal ion–dependent adhesion site (MIDAS). Drugs patterned on the integrin ligand sequence Arg-Gly-Asp have a basic moiety that binds the α_{IIb} subunit and a carboxyl group that coordinates the MIDAS Mg^{2+} in the β_3 subunits. They induce conformational changes in the β_3 subunit that may have negative consequences such as exposing previously hidden epitopes and inducing the active conformation of the receptor. We recently reported an inhibitor of $\alpha_{IIb}\beta_3$ (RUC-1) that binds exclusively to the α_{IIb} subunit; here, we report the structure-based design and synthesis of RUC-2, a RUC-1 derivative with a ~100-fold higher affinity. RUC-2 does not induce major conformational changes in β_3 as judged by monoclonal antibody binding, light scattering, gel chromatography, electron microscopy, and a receptor priming assay. X-ray crystallography of the RUC-2–$\alpha_{IIb}\beta_3$ headpiece complex in 1 mM calcium ion (Ca^{2+})/5 mM Mg^{2+} at 2.6 Å revealed that RUC-2 binds to α_{IIb} the way RUC-1 does, but in addition, it binds to the β_3 MIDAS residue glutamic acid 220, thus displacing Mg^{2+} from the MIDAS. When the Mg^{2+} concentration was increased to 20 mM, however, Mg^{2+} was identified in the MIDAS and RUC-2 was absent. RUC-2's ability to inhibit ligand binding and platelet aggregation was diminished by increasing the Mg^{2+} concentration. Thus, RUC-2 inhibits ligand binding by a mechanism different from that of all other $\alpha_{IIb}\beta_3$ antagonists and may offer advantages as a therapeutic agent.

INTRODUCTION

Integrin receptors are heterodimeric complexes composed of α and β subunits that bind ligand and transduce signals bidirectionally (*1*, *2*). They contribute to many different biologic and pathologic processes, including hemostasis, thrombosis, angiogenesis, immunity, development, bone resorption, and metastases (*3*–*7*). The platelet $\alpha_{IIb}\beta_3$ receptor is a validated therapeutic target, with three separate agents that inhibit ligand binding to the receptor (abciximab, eptifibatide, and tirofiban) approved for human use. These have shown clinical benefit in controlled trials in selected high-risk patients when used as adjunctive therapy to prevent ischemic complications of percutaneous coronary interventions and in other clinical conditions (*8*). The current agents have several limitations, however, including the need for intravenous administration and the induction of thrombocytopenia in some patients (*9*, *10*). A number of oral $\alpha_{IIb}\beta_3$ antagonists patterned after the Arg-Gly-Asp (RGD) integrin binding sequence have been developed, but none have achieved regulatory approval because they were not efficacious when used as chronic therapy (*11*). Treatment with several of the agents was associated with an increased risk of death (*11*, *12*), as well as with thrombocytopenia and an increased risk of bleeding in a small percentage of patients (*13*). Both the increased risk of death associated with the oral agents and the thrombocytopenia associated with both the intravenous and the oral agents have been hypothesized to result, at least in part, from conformational changes in the receptor induced by the binding of the agents (*9*, *10*, *13*–*20*).

On the basis of electron microscopy (EM) and x-ray crystallography studies, the two best documented conformational changes in the receptor are headpiece extension and headpiece opening, in which the β_3 hybrid domain swings away from the α_{IIb} β-propeller domain at its junction with the β_3 βI domain (*21*–*24*). This latter movement is linked with remodeling of the β_3 βI domain at the ligand-binding pocket formed at its interface with the α_{IIb} subunit β-propeller domain. Crystal structures of the $\alpha_{IIb}\beta_3$ binding pocket in complex with eptifibatide, tirofiban, and other RGD-based antagonists, as well as the binding of the fibrinogen γ-chain C-terminal peptide, have identified a common binding mechanism involving binding to Asp^{224} in α_{IIb} via the compound's Arg (or its equivalent basic or Lys moiety) and coordinating the metal ion–dependent adhesion site (MIDAS) Mg^{2+} ion in the β_3 subunit via one of the oxygen atoms in the compound's Asp carboxyl or an equivalent carboxyl (*22*, *23*). The binding of these agents was associated with the receptor adopting the β_3 swing-out conformation as judged by x-ray crystallography (*23*). Because very early treatment of myocardial infarction with $\alpha_{IIb}\beta_3$ antagonists can prevent cardiac damage (*25*–*27*), it would be desirable to have an orally active agent that inhibits the receptor but does not induce the global conformational changes in the receptor.

We recently reported on a small-molecule inhibitor of $\alpha_{IIb}\beta_3$ termed RUC-1 (Fig. 1) that was identified by high-throughput screening with an assay based on the adhesion of platelets to immobilized fibrinogen

[1]Immune Disease Institute, Children's Hospital Boston, and Department of Pathology, Harvard Medical School, Boston, MA 02115, USA. [2]BloodCenter of Wisconsin, Medical College of Wisconsin, Milwaukee, WI 53201, USA. [3]Laboratory of Blood and Vascular Biology, Rockefeller University, New York, NY 10065, USA. [4]NIH Chemical Genomics Center, National Center for Advancing Translational Sciences, National Institutes of Health, Bethesda, MD 20892, USA. [5]Department of Structural and Chemical Biology, Mount Sinai School of Medicine, New York, NY 10029, USA.
*These authors contributed equally to this work.
†To whom correspondence should be addressed. E-mail: collerb@rockefeller.edu

(*28*, *29*). RUC-1 is specific for $\alpha_{IIb}\beta_3$ relative to $\alpha_V\beta_3$, $\alpha_2\beta_1$, and glycoprotein Ib (GPIb) and has antithrombotic effects in murine models in both large and small blood vessels when administered at 25.6 mg/kg. RUC-1 differs from the RGD-based $\alpha_{IIb}\beta_3$ antagonists eptifibatide and tirofiban in producing less extensive exposure of β_3 ligand–induced binding sites as detected by monoclonal antibodies (mAbs), suggesting that it also produces less extensive conformational changes in the β_3 subunit (*28*). Computer-assisted molecular docking studies corroborated by molecular dynamic (MD) simulations suggested that RUC-1 binds exclusively to the α_{IIb} subunit, providing a potential explanation for its reduced ability to expose β_3 ligand–induced binding sites (*28*–*30*). Subsequent studies in which RUC-1 was soaked into crystals of the $\alpha_{IIb}\beta_3$ headpiece confirmed that it binds exclusively to α_{IIb} and, thus, unlike the RGD-based compounds, does not coordinate the β_3 MIDAS metal ion (*30*). RUC-1 also does not initiate the reorganization of the β_3 metal ions that is associated with the binding of RGD-based antagonists and the adoption of the β_3 swing-out orientation. Additional gel permeation and dynamic light scattering (DLS) studies demonstrated that, unlike eptifibatide and tirofiban, RUC-1 does not induce conformational changes detectable by these techniques (*30*).

To further explore the $\alpha_{IIb}\beta_3$ binding pocket and obtain additional information on the correlation between binding mechanism and induction of conformational changes in the receptor, we synthesized a series of derivatives of RUC-1 guided by structural and energetic considerations. One of these, termed RUC-2 (Fig. 1A and fig. S1), was more than 100 times more potent in inhibiting platelet aggregation than RUC-1, and so it was selected for further evaluation.

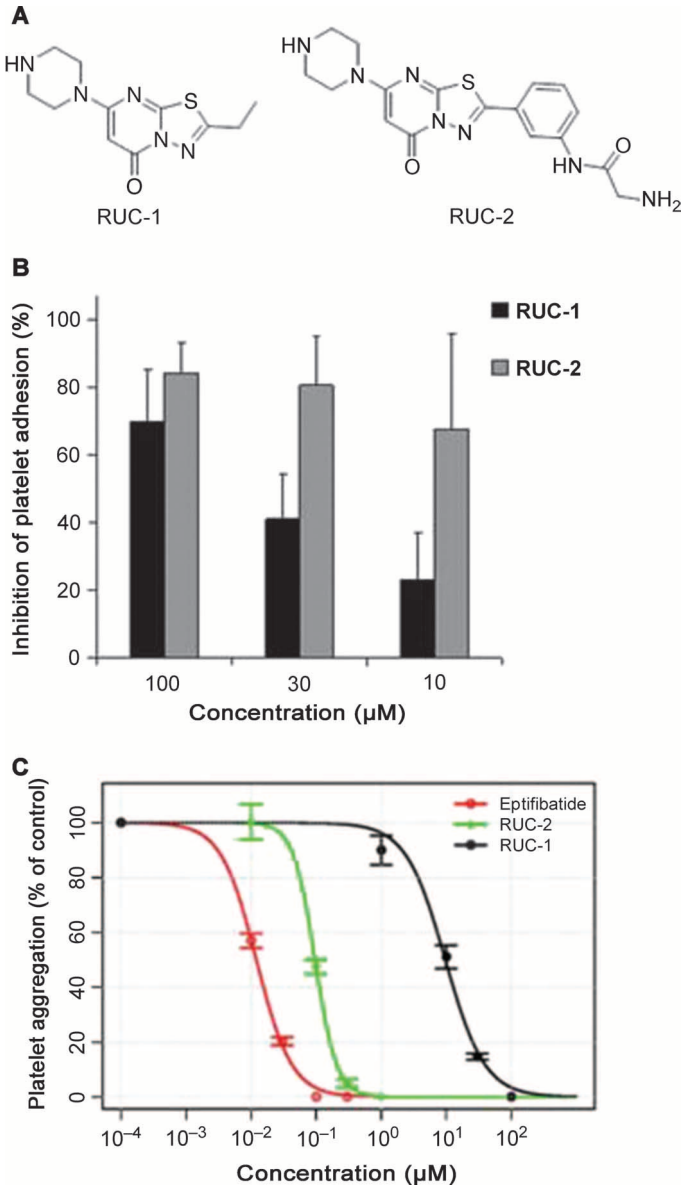

Fig. 1. Chemical structure of RUC-2 and effects on platelet adhesion and aggregation. (**A**) Chemical structures of RUC-1 (left) and RUC-2 (right). (**B**) Effect of RUC-1 and RUC-2 on platelet adhesion to immobilized fibrinogen. RUC-1 and RUC-2 were tested at the indicated concentrations. Data are means ± SD and $n = 5$. (**C**) Effect of RUC-1, RUC-2, and eptifibatide on platelet aggregation induced by ADP. Citrated PRP was incubated with either RUC-1, RUC-2, or eptifibatide at the indicated concentrations for 15 min, and then aggregation was induced by adding ADP (5 μM). The initial slope of aggregation was measured, and the inhibition was assessed as a percentage of the aggregation in the absence of an $\alpha_{IIb}\beta_3$ antagonist (designated as a concentration of $10^{-\infty}$). The IC_{50} for RUC-2 (96 ± 5 nM) was more than two logs lower than the IC_{50} for RUC-1 (9.7 ± 1 μM) and nearly a log higher than the IC_{50} for eptifibatide (12 ± 1 nM).

RESULTS

RUC-2's chemical and biologic properties are summarized in Table 1.

Platelet adhesion screening assay

In five separate experiments, RUC-2 produced 83 ± 7% (mean ± SD) inhibition of platelet adhesion to fibrinogen at a concentration of 100 μM, 80 ± 13% inhibition at 30 μM, and 66 ± 10% inhibition at 10 μM (Fig. 1B); the comparable values for RUC-1 at the same concentrations were 70 ± 15%, 38 ± 10%, and 22 ± 8%. For further comparison, tirofiban produced 87 ± 9% inhibition at 10 μM.

Platelet aggregation: Human platelets

RUC-2 inhibited adenosine diphosphate (ADP)–induced platelet aggregation of citrated platelet-rich plasma (PRP) with an IC_{50} (the concentration of a substance required to inhibit the activity of another substance by 50%) of 96 ± 5 nM ($n = 4$) (Fig. 1C). By comparison, RUC-1's IC_{50} was more than two logs higher, at 9.7 ± 1.0 μM. For comparison, the IC_{50} for eptifibatide was 12 ± 1 nM when tested on the same PRP samples. When PPACK (Phe-Pro-Arg chloromethyl ketone) was used as the anticoagulant instead of citrate, the IC_{50} for RUC-2 was more than twofold higher (220 nM; $n = 4$).

Platelet aggregation: Mouse and rat platelets

At doses that nearly completely inhibited human platelet aggregation, RUC-2 (1 μM), like RUC-1 (100 μM), did not inhibit either mouse or rat platelet aggregation induced by ADP (fig. S2, A and B). In contrast, RUC-2 essentially completely inhibited the aggregation of platelets from a mouse expressing human α_{IIb} and mouse β_3 (hαIIb/mβ3) (fig. S2C).

Platelet adhesion/aggregation to collagen

Consistent with our previous reports (*28*, *31*), the anti-$\alpha_2\beta_1$ mAb 6F1 produced 95% inhibition of platelet adhesion/aggregation to collagen,

whereas the anti-$\alpha_{IIb}\beta_3$ mAb 10E5 and the anti-$\alpha_{IIb}\beta_3$ + $\alpha_V\beta_3$ mAb 7E3 produced ~30% inhibition (fig. S3). RUC-2 at 1 to 100 μM also inhibited adhesion/aggregation by ~30%, and combining RUC-2 with the anti-$\alpha_{IIb}\beta_3$ antibody 10E5 did not further inhibit adhesion/aggregation. Microscopic analysis indicated that, as reported with RUC-1 and the anti-mAb 10E5, RUC-2 did not decrease platelet adhesion to collagen, but decreased the recruitment of additional platelets to the adherent platelets.

$\alpha_V\beta_3$-mediated cell adhesion to vitronectin and $\alpha_{IIb}\beta_3$-mediated cell adhesion to fibrinogen

The $\alpha_V\beta_3$-specific mAb LM609 inhibited adhesion of human embryonic kidney (HEK) 293 cells expressing $\alpha_V\beta_3$ to vitronectin by 74 ± 27% (n = 4) at 20 μg/ml, and the anti-$\alpha_V\beta_3$ + $\alpha_{IIb}\beta_3$ mAb 7E3 inhibited adhesion by 80 ± 12% (n = 4) at 40 μg/ml (fig. S4A). In contrast, RUC-1 at 100 μM produced only 5 ± 7% (n = 4) inhibition and RUC-2 at 10 μM produced only 6 ± 15% (n = 4). The RUC-1 and RUC-2 data are both similar to the 2 ± 9% (range, −9.4 to +7.6%) (n = 3) inhibition produced by the $\alpha_{IIb}\beta_3$-specific mAb 10E5.

Table 1. Properties of RUC-2, 2-amino-*N*-(3-(5-oxo-7-(piperazin-1-yl)-5*H*-[1,3,4]thiadiazolo[3,2-a]pyrimidin-2-yl)phenyl)acetamide (NCGC00183896-01) (ML165).

Category	Parameter	Description
Compound	Citation	
	Name	(RUC-2) (NCGC00183896-01) (ML165)
	Chemical descriptors	
	Molecular weight	385.443 g/mol
	Entries in chemical databases	PubChem: CID 44820665, SID 8944968
	Additional comments	pK_a values by titration in water: 6.41 and 8.08
In vitro profiling	Target	$\alpha_{IIb}\beta_3$ receptor
	Potency	96 ± 5 nM in ADP-induced platelet aggregation assay
	Selectivity	6 ± 15% inhibition of ligand binding to the $\alpha_V\beta_3$ receptor.
	SAR	A manuscript detailing the SAR is in preparation.
	Mechanism of inhibition	Orthosteric inhibition at the RGD binding domain as determined by x-ray crystallography
	Structure of target-probe complex	PDB code 3T3M
Cellular profiling	Validation of cellular target	RUC-2 inhibited $\alpha_{IIb}\beta_3$-dependent platelet adhesion to fibrinogen in a screening assay and $\alpha_{IIb}\beta_3$-dependent platelet aggregation. It was found to bind to the target via x-ray crystallography (PDB code 3T3M).
	Validation of cellular specificity	RUC-2 had minimal effect on $\alpha_V\beta_3$-mediated cell adhesion to vitronectin.

LM609 did not inhibit the adhesion of HEK293 cells expressing $\alpha_{IIb}\beta_3$ to fibrinogen (fig. S4B), whereas 10E5 produced 79 ± 10% inhibition, 7E3 produced 87 ± 9% inhibition, RUC-1 produced 55 ± 5% inhibition, and RUC-2 produced 65 ± 5% inhibition (all n = 4) at the same concentrations indicated for the $\alpha_V\beta_3$ experiments.

Induction of ligand-induced binding site epitopes

Two different β_3 ligand–induced binding site antibodies were tested, AP5 and LIBS1, which bind to the PSI (plexin-semaphorin-integrin) domain and the distal leg region, respectively (*32*, *33*). The net normalized fluorescence intensity in the presence of eptifibatide (10 μM, 30-min incubation at 22°C) was assigned the value of 100%. Untreated platelets bound 7 ± 3% (n = 5) of the amount of AP5 bound in the presence of eptifibatide (fig. S5). In the presence of RUC-1, platelets bound 10 ± 4% of the amount of AP5 bound in the presence of eptifibatide, and in the presence of RUC-2, they bound 18 ± 5%. The comparable data for LIBS1 binding after 30 min were 22 ± 3% (n = 5) for untreated platelets, 18 ± 2% for platelets in the presence of RUC-1, and 21 ± 3% for platelets in the presence of RUC-2. The α_{IIb} LIBS antibody PMI-1 was also tested (*34*). Untreated platelets bound 46 ± 5% (n = 4) of the amount of PMI-1 that platelets treated with eptifibatide bound; both RUC-1 and RUC-2 increased PMI-1 binding to similar extents (73 ± 9 and 82 ± 13%, respectively).

Effect of RUC-1 and RUC-2 on recruitment of $\alpha_{IIb}\beta_3$-dependent antibodies to platelets

Sera from 20 patients who developed thrombocytopenia after treatment with the RGD-mimetic platelet inhibitors tirofiban (5 cases) or eptifibatide (15 cases) were studied for reactivity with normal human platelets pretreated with tirofiban (4.0 μM), eptifibatide (2.4 μM), RUC-1 (100 μM), RUC-2 (3.9 μM), or, as a control, a structurally related derivative of RUC-1 that does not inhibit ligand binding. In accord with our previous studies (*9*), pretreatment of platelets with either tirofiban or eptifibatide enhanced recruitment of immunoglobulin G (IgG) to the platelet surface from the sera of all of the patients. The strength of these reactions, as judged by median fluorescence intensity (MFI), ranged from 2.2 to 54 (median, 8.0) times the strength of the reactions obtained with control platelets treated with the inactive derivative of RUC-1. Neither RUC-1 nor RUC-2 induced recruitment of patient IgG to platelets when tested with all 5 tirofiban samples and 13 of 15 eptifibatide samples. Two sera from patients who experienced eptifibatide-induced thrombocytopenia recognized platelets treated with RUC-1 or RUC-2. One of these produced median MFI values with RUC-1– and RUC-2–treated platelets that were 6.8 and 4.2 times greater than the signals obtained with control platelets, but these increases were only 13 and 8%, respectively, of the values obtained with eptifibatide-treated platelets. The second recognized platelets pretreated with RUC-2, but not RUC-1, producing a signal that was 14 times the signal obtained with control platelets and 1.4 times the signal obtained with the eptifibatide-treated platelets. These two eptifibatide-treated patient samples were also unusual in that both tirofiban and the peptide RGDW were able to recruit patient IgG.

Effect of RUC-2 on extension of purified $\alpha_{IIb}\beta_3$ as judged by EM

In accord with the data of Ye *et al.* (*35*), in the absence of compounds, $\alpha_{IIb}\beta_3$ primarily adopted a compact conformation adjacent to the nanodisc (Fig. 2), giving nanodisc-integrin length (NIL) values primarily

between 11 and 17 nm (Fig. 2, A, B, and E). Occasional nanodiscs, however, contained $\alpha_{IIb}\beta_3$ molecules that were extended, giving NIL values between 18 and 23. As a result, the NIL frequency distribution showed a bimodal pattern, with a marked predominance of $\alpha_{IIb}\beta_3$ nanodiscs in the range of 11 to 17 nm, and a small subpopulation in the range 18 to 23 nm (Fig. 2, B and E). Both eptifibatide and tirofiban shifted the distribution in a dose-dependent manner such that, at the highest doses, most $\alpha_{IIb}\beta_3$ nanodiscs had NIL values in the range of 18 to 23 nm (Fig. 2, A and C to E) ($P < 0.001$ and $P < 0.001$, respectively). In contrast, neither RUC-1 at concentrations up to 100 μM nor RUC-2 at concentrations up to 10 μM produced a significant shift in NIL values ($P = 0.23$ and 0.37, respectively) (Fig. 2, A, B, and E).

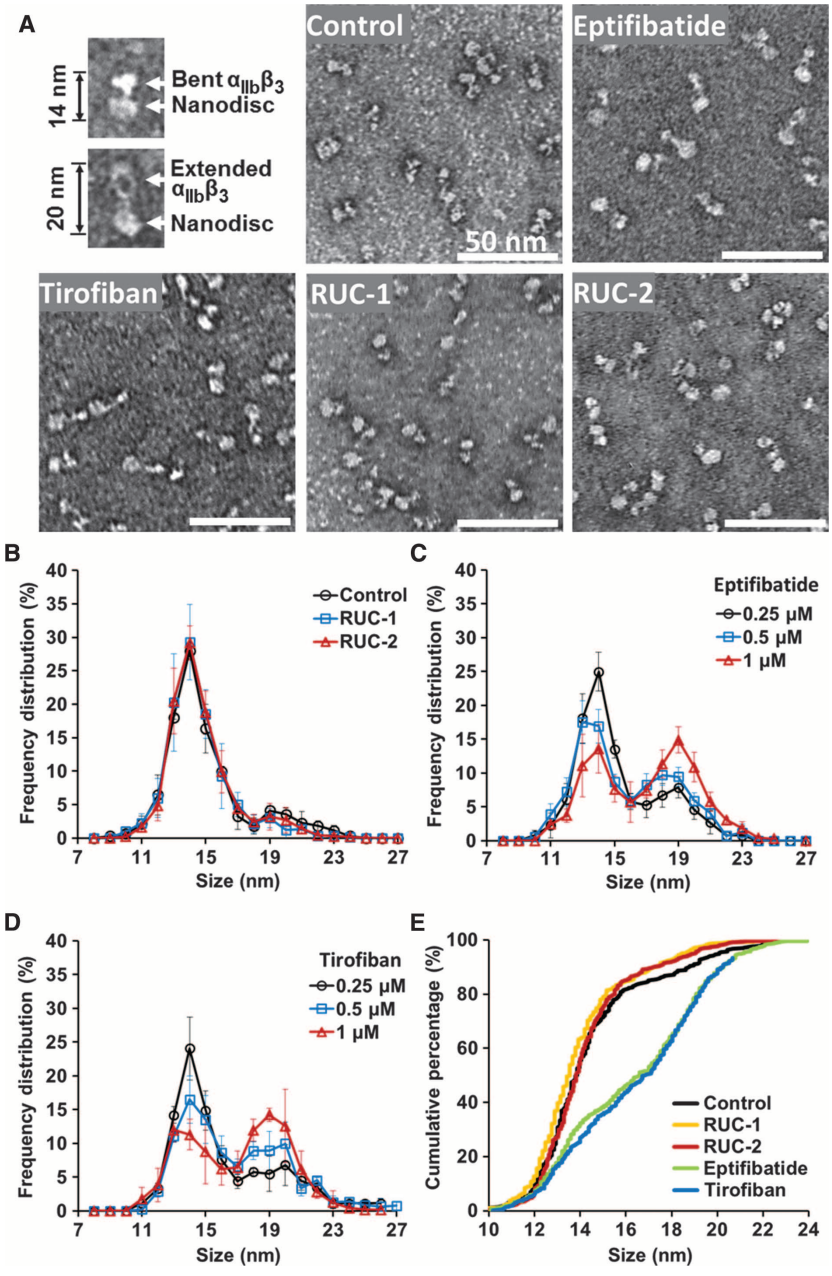

Fig. 2. Negative stain EM of $\alpha_{IIb}\beta_3$ nanodiscs in the absence and presence of $\alpha_{IIb}\beta_3$ antagonists. (**A**) Representative images of bent and extended $\alpha_{IIb}\beta_3$ nanodiscs and images of $\alpha_{IIb}\beta_3$ nanodiscs in the presence of buffer, eptifibatide (1 μM), tirofiban (1 μM), RUC-1 (100 μM), or RUC-2 (10 μM). (**B** to **D**) Quantitative measurements of $\alpha_{IIb}\beta_3$ NIL values in the absence and presence of $\alpha_{IIb}\beta_3$ antagonists. (B) NIL value distributions in the presence of buffer, 100 μM RUC-1, or 10 μM RUC-2. (C and D) Dose-dependent NIL value distributions in the presence of eptifibatide (C) or tirofiban (D). The mean ± SD of five separate experiments is depicted for each condition; a total of 600 to 700 particles contained in five separate electron microscopic images were measured at ×33,000 magnification in each experiment. (**E**) Cumulative percentage of NIL values in the presence of buffer, 100 μM RUC-1, 10 μM RUC-2, 1 μM eptifibatide, or 1 μM tirofiban.

Effect of RUC-2 on the Stokes radius of the soluble $\alpha_{IIb}\beta_3$ headpiece

We examined the effect of RUC-2 on the conformation of the $\alpha_{IIb}\beta_3$ headpiece in solution by gel filtration or DLS with or without near-saturating concentrations of RUC-1, RUC-2, or tirofiban. Consistent with our previous results (*30*), gel filtration showed that tirofiban induced a substantial reduction in the $\alpha_{IIb}\beta_3$ headpiece elution volume (0.38 ml) (Fig. 3A). In contrast, RUC-2 and RUC-1 had little effect on elution volume of the $\alpha_{IIb}\beta_3$ headpiece (0.07 and 0.03 ml, respectively) (Fig. 3A). These changes in elution volumes corresponded to a 0.4-nm increase in Stokes radius with tirofiban, and little or no increases with RUC-1 or RUC-2 (Fig. 3B). When measured by DLS, a similar increase in Stokes radius was found with tirofiban (0.45 nm). RUC-1 and RUC-2 produced considerably smaller but measurable increases in Stokes radius (0.08 and 0.16 nm, respectively) (Fig. 3B). These results suggest that RUC-2 induces less opening of the $\alpha_{IIb}\beta_3$ headpiece in solution than tirofiban.

Effect of RUC-2 on $\alpha_{IIb}\beta_3$ high-affinity ligand-binding conformation

Because small-molecule $\alpha_{IIb}\beta_3$ antagonists based on the RGD motif induce a high-affinity ligand-binding conformation in $\alpha_{IIb}\beta_3$ (*16*, *20*, *36*–*38*), and because this activity has been proposed to explain the paradoxical increase in thrombotic death associated with the small-molecule oral $\alpha_{IIb}\beta_3$ antagonists (*11*, *12*, *14*, *18*, *37*), we tested the "priming" effect of RUC-2, that is, its ability to induce fibrinogen binding to platelet $\alpha_{IIb}\beta_3$. Incubation of washed platelets with eptifibatide (1 μM), tirofiban (0.5 μM), or an RGDS peptide (100 μM), followed by fixation in paraformaldehyde and washing, increased the binding of

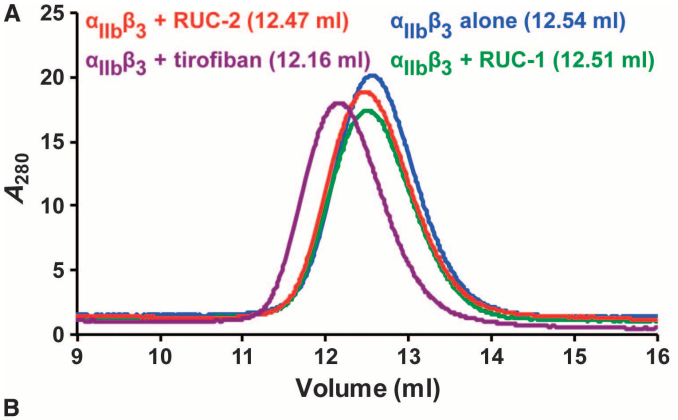

B

Stokes radii measured by gel filtration or dynamic light scattering (DLS)

	Gel filtration	DLS
$\alpha_{IIb}\beta_3$ headpiece alone	4.83 ± 0.04 nm	4.66 ± 0.07 nm
$\alpha_{IIb}\beta_3$ headpiece + RUC-1	4.82 ± 0.01 nm	4.74 ± 0.05 nm
$\alpha_{IIb}\beta_3$ headpiece + RUC-2	4.86 ± 0.03 nm	4.82 ± 0.03 nm
$\alpha_{IIb}\beta_3$ headpiece + tirofiban	5.23 ± 0.02 nm	5.11 ± 0.05 nm

Fig. 3. Stokes radius determinations by gel filtration and DLS. (**A**) Gel filtration profile of $\alpha_{IIb}\beta_3$ headpiece alone or bound with antagonists. The untagged $\alpha_{IIb}\beta_3$ headpiece was mixed with near-saturating concentrations of RUC-1, RUC-2, or tirofiban and incubated at room temperature for 1 hour before chromatography on Superdex 200 in tris-buffered saline plus 1 mM Ca^{2+}/Mg^{2+}. The elution volumes are shown in parentheses. (**B**) Stokes radii calculated from gel filtration or DLS. Data are means ± SD (n = 2 for gel filtration; n = 3 for DLS).

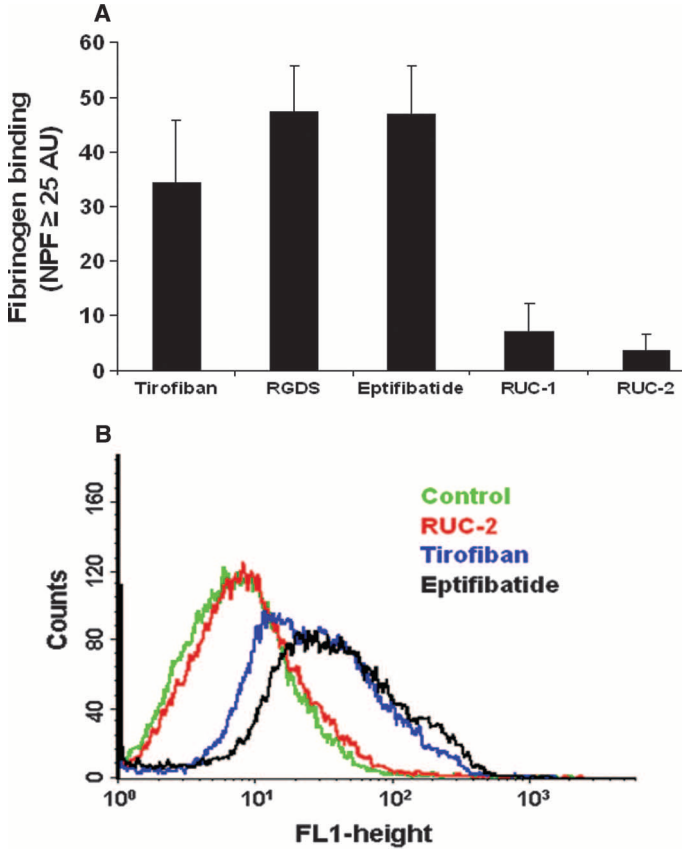

Fig. 4. Effect of RUC-2 on priming platelets to bind fibrinogen. Washed platelets were incubated with eptifibatide (1 μM), tirofiban (0.5 μM), RGDS (100 μM), RUC-1 (100 μM), or RUC-2 (1 μM) for 20 min and fixed with 1% paraformaldehyde for 40 min. After the paraformaldehyde was quenched with glycine (5 mM), platelets were washed and incubated with fluorescent fibrinogen (200 μg/ml) in the presence of 2 mM Ca^{2+} and 1 mM Mg^{2+}. After washing, the platelets were analyzed by flow cytometry. (**A**) Mean ± SD (n = 4) net platelet fluorescence (NPF), defined as the percentage of platelets with fluorescence intensity values above 25 arbitrary units (AU) in the presence of one of the antagonists minus the percentage in the absence of the antagonist. Eptifibatide blocked the binding of fibrinogen induced by the antagonists, yielding values equal to or below the control value. (**B**) Fluorescence data from one of the four similar experiments.

fluorescent fibrinogen to platelets as judged by the percentage of platelets with fluorescence values above those in the absence of the agents. The values were 47 ± 9, 34 ± 12, and 48 ± 8% (n = 4), respectively (Fig. 4). In contrast, the value for RUC-1 (100 μM) was only 8 ± 3% (n = 4), and for RUC-2 (1 μM), it was only 4 ± 3% (n = 4). Increasing the RUC-2 concentration to 5 μM, more than 20-fold its IC_{50}, did not increase the fibrinogen binding. The specificity of the fibrinogen binding induced by the agents was established by the ability of eptifibatide to block the binding when present during the fibrinogen binding step [for example, in one experiment, the incremental fibrinogen binding values for eptifibatide (34%), tirofiban (17%), the RGDS peptide (36%), and RUC-1 (2%) were all reduced by eptifibatide to 0%; RUC-2 did not produce any incremental binding in this experiment].

Mechanism of RUC-2 binding to $\alpha_{IIb}\beta_3$ as revealed by crystallography

An $\alpha_{IIb}\beta_3$ headpiece–Fab complex was crystallized in the closed headpiece conformation (*30*). We obtained a diffraction data set to 2.6 Å from a crystal soaked with RUC-2 in 1 mM Ca^{2+} and 5 mM Mg^{2+} (Table 2). Clear electron densities for RUC-2 and Ca^{2+} ions at the synergy metal binding site (SyMBS) and the adjacent to MIDAS metal binding site (ADMIDAS) were found at the RGD-binding pocket in each of the two crystallographically independent molecules in the asymmetric unit (Fig. 5A). However, we saw no density for a metal ion at the MIDAS (Fig. 4A). Compared to the native structure (*21*, *30*) or the structure of the RUC-1 complex (*30*), soaking RUC-2 into the crystal did not induce any significant change in the α_{IIb} or β_3 subunits, except for the absence of the Mg^{2+} ion at the MIDAS (Fig. 5A). To test for competition between RUC-2 and Mg^{2+}, we also obtained 2.2 and 2.4 Å diffraction data sets from crystals soaked with RUC-2 in the presence of 1 mM Ca^{2+} and 20 mM Mg^{2+}. Clear electron densities of Ca^{2+} ions at the SyMBS and ADMIDAS, as well as a Mg^{2+} ion at the MIDAS, were found in both crystals, but no densities of RUC-2 were visible in either of the two independent molecules in the asymmetric unit in the crystals (fig. S6). Instead, the ligand-binding pocket was occupied by water molecules.

RUC-2 fits into the same binding pocket in the α_{IIb} β-propeller domain as RUC-1, which is lined with residues Phe^{160}, Tyr^{190}, Leu^{192}, Asp^{224}, Phe^{231}, and Asp^{232} (Fig. 5, B and C). RUC-2 maintains the same interactions as seen with RUC-1, including the hydrogen bonding with α_{IIb} Asp^{224}, the π-π stacking interaction with α_{IIb} Tyr^{190}, and the water-mediated hydrogen bonding with α_{IIb} Asp^{232} (Fig. 5, B and C).

Table 2. Statistics of x-ray diffraction data and structure refinement. RMSD, root mean square deviation.

Ligand	RUC-2 (1 mM Ca/5 mM Mg)	RUC-2 (1 mM Ca/20 mM Mg)
Space group	$P2_12_12$	$P2_12_12$
Unit cell		
(*a*, *b*, *c*) (Å)	261.2, 145.3, 104.7	259.5, 145.3, 104.8
(α, β, γ) (°)	90, 90, 90	90, 90, 90
Wavelength (Å)	1.0331	1.0332
Resolution (Å)	50–2.6/2.74–2.60*	50–2.2/2.32–2.20*
Number of reflections (total/unique)	743,660/118,868	1,236,472/199,292*
Completeness (%)	96.7/92.3*	99.3/96.2*
$I/\sigma(I)$	6.2/1.8*	13.4/1.6*
R_{merge} (%)†	17.6/89.7*	8.1/102.5*
R_{work}‡/R_{free}§	0.179/0.222	0.189/0.220
RMSD		
Bond (Å)	0.006	0.009
Angle (°)	0.696	0.850
Ramachandran plot‖	95.0%/4.7%/0.3%	95.8%/4.0%/0.2%
Molecules per asymmetric unit	2	2
Residues, α_{IIb}/β_3	1–454 (453)/1–466 (471)¶	1–454 (453)/1–466 (471)¶
Non-H atoms, protein/carbohydrate/water	20,770/195/855	20,866/195/1,291
PDB code	3T3M	3T3P

*Numbers correspond to the last resolution shell. †$R_{merge} = \Sigma_h\Sigma_i|I_i(h) - \langle I(h)\rangle|/\Sigma_h\Sigma_i I_i(h)$, where $I_i(h)$ and $\langle I(h)\rangle$ are the *i*th and mean measurement of the intensity of reflection *h*. ‡$R_{work} = \Sigma_h||F_{obs}(h)| - |F_{calc}(h)||/\Sigma_h|F_{obs}(h)|$, where $F_{obs}(h)$ and $F_{calc}(h)$ are the observed and calculated structure factors, respectively. No *I*/*s* cutoff was applied. §R_{free} is the *R* value obtained for a test set of reflections consisting of a randomly selected 0.86 or 0.5% subset of data excluded from refinement. ‖Residues in favorable, allowed, and outlier of the Ramachandran plot as reported by MolProbity. ¶Numbers in parentheses correspond to chains C and D.

In addition to the interactions with α_{IIb}, RUC-2 makes direct contacts with the β_3 βI domain. Its primary amine group forms hydrogen bonds with one of the oxygens of the β_3 Glu^{220} carboxyl side chain and with the carbonyl oxygen of β_3 Ala^{218} through a water molecule (Fig. 5B). In addition, RUC-2's phenylacetamide nitrogen forms a hydrogen bond with the carbonyl oxygen of β_3 Asn^{215}. The phenyl group in RUC-2 that replaces the ethyl group in RUC-1 also increases hydrophobic interactions with the binding pocket. These additional interactions with the β_3 subunit can account for the higher affinity of RUC-2 compared with RUC-1.

Like the RGD-mimetic drug tirofiban, RUC-2's Arg-mimetic piperazinyl group interacts with α_{IIb} Asp^{224}. However, RUC-2 lacks an Asp-mimetic terminal carboxyl group with which to interact with the MIDAS Mg^{2+} ion and the backbone nitrogen atoms of the MIDAS residues Tyr^{122} and Ser^{123} (Fig. 5, B and D). Instead, RUC-2 has a terminal primary amine group that interacts directly with the side-chain oxygen of Glu^{220} that ordinarily contributes to coordinating the MIDAS Mg^{2+} ion. The absence of the MIDAS Mg^{2+} metal ion in the presence of RUC-2 thus likely reflects the loss of metal ion coordination by the Glu^{220} carboxyl oxygen, steric hindrance, and/or electrostatic repulsion (Fig. 5B). When a higher concentration of Mg^{2+} was used (20 mM) during crystal soaking, we identified the Mg^{2+} but not RUC-2 (fig. S6), suggesting that RUC-2 competes with Mg^{2+} for interaction with Glu^{220}.

Molecular docking and MD simulations

A single RUC-1–like docking pose of RUC-2 was identified in the absence of the MIDAS Mg^{2+} ion, regardless of whether the primary amine was uncharged or positively charged, and this pose remained stable throughout 10 ns of MD simulation (fig. S7). As inferred from the crystal structure, the primary amine group of RUC-2 interacted directly with the carboxyl oxygen of the β_3 Glu^{220} residue regardless of whether the RUC-2 primary amine was uncharged (fig. S7, A and C) or positively charged (fig. S7, B and D). The interaction remained stable in both simulations with slightly different relative average distances (~3.5 Å versus ~2.8 Å, respectively).

Mg^{2+} effects on the IC_{50} of RUC-2, RUC-1, and tirofiban

Both crystallographic and computational data supported a model in which RUC-2 and Mg^{2+} compete for binding to the same Glu^{220} carboxyl oxygen. To test this hypothesis, we assessed the binding of the ligand-mimetic mAb PAC-1 to Chinese hamster ovary (CHO) cells expressing recombinant human $\alpha_{IIb}\beta_3$ after activation with the mAb PT25-2 at different Mg^{2+} concentrations (Fig. 6, A to D). In going from 1 to 50 mM Mg^{2+}, the RUC-2 IC_{50} increased by ~3.9-fold, reflecting nearly a 75% reduction in affinity. In contrast, the IC_{50} of RUC-1 was increased by only ~6% and that of tirofiban was completely unchanged. Thus, as predicted from the structural studies, higher Mg^{2+} concentrations can decrease RUC-2's inhibition of ligand binding.

To further test the effects of varying the Mg^{2+} concentration on RUC-2's ability to inhibit $\alpha_{IIb}\beta_3$ ligand binding, we performed the platelet adhesion to fibrinogen assay at different Mg^{2+} concentrations, keeping the Ca^{2+} concentration at 1 mM. In three separate experiments, the IC_{50} for RUC-2 increased from 0.29 ± 0.1 μM (mean ± SD) at 1 mM Mg^{2+} to 0.91 ± 0.21 μM at 20 mM Mg^{2+} ($P < 0.01$) and to 1.3 ± 0.35 μM at 50 mM Mg^{2+} ($P < 0.01$) (Fig. 6, E to G). Thus, in

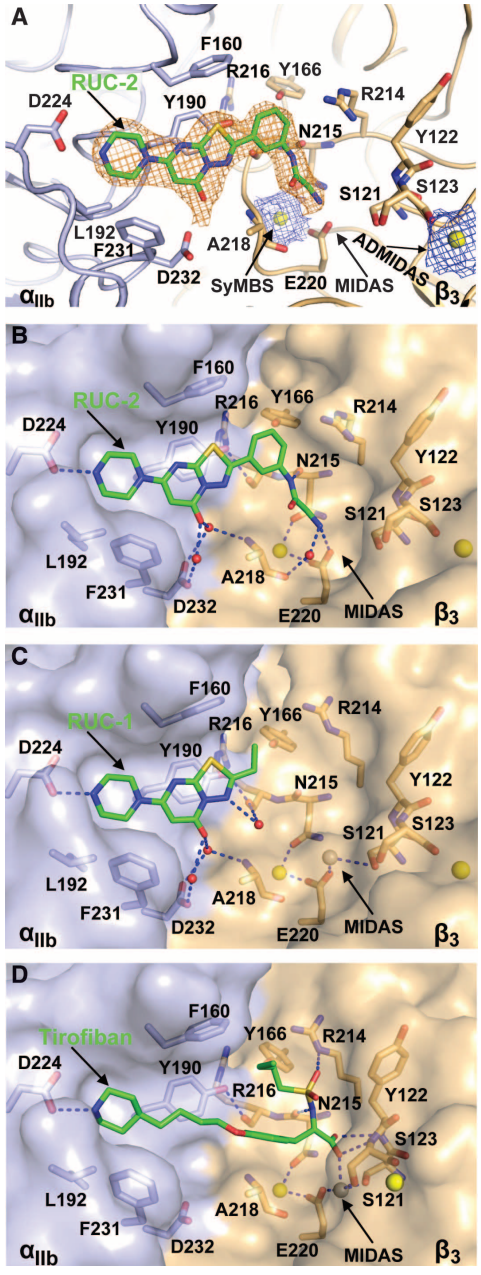

Fig. 5. The binding pocket of RUC-2 in the closed $\alpha_{IIb}\beta_3$ headpiece crystal structure. (**A**) Electron density maps of RUC-2 and metal ions. α_{IIb} β-propeller (light blue) and β_3 βI (wheat) domains are shown as cartoon. Ca^{2+} ions of the SyMBS and ADMIDAS are shown as yellow spheres. RUC-2 and selected $\alpha_{IIb}\beta_3$ side-chain and backbone atoms are shown as sticks with green (RUC-2), light blue (αIIb), or wheat carbon (β3), red oxygen, blue nitrogen, and yellow sulfur atoms. $2F_{obs} - F_{calc}$ maps at 1.5 σ for RUC-2 and Ca^{2+} ions are shown in orange and blue, respectively. (**B** to **D**) Comparison of RUC-2, RUC-1 (PDB code 3NIF), and tirofiban (PDB code 2VDM) binding modes. Color code is the same as in (A). α_{IIb} and β_3 are shown as solvent-accessible surfaces. Ca^{2+} ions of SyMBS or ADMIDAS (yellow) and the Mg^{2+} ion of MIDAS (silver) are shown as spheres. Water molecules are small red spheres. Hydrogen and metal coordination bonds are shown as blue dashed lines. The RUC-1 and tirofiban structures are after superposition on the RUC-2 complex using super command in PyMOL with the α_{IIb} β-propeller and β_3 βI domains.

going from 1 to 50 mM Mg^{2+}, there was an ~4.5-fold increase in IC_{50}, corresponding to ~80% decrease in affinity. Neither RUC-1 nor tirofiban showed a comparable increase in IC_{50} at higher Mg^{2+} concentrations. Finally, we tested the effect of RUC-2 (1 μM) and RUC-1 (100 μM) on platelet aggregation induced by a thrombin receptor–activating peptide (SFLLRN) at different Mg^{2+} concentrations and observed that the inhibitory effect of RUC-2 was clearly attenuated at 20 mM Mg^{2+}, whereas the effect on RUC-1 was much less evident (Fig. 6H).

DISCUSSION

We previously demonstrated that a small, α_{IIb}-specific compound (RUC-1) could effectively inhibit ligand binding, platelet aggregation, and in vivo thrombus formation mediated by human $\alpha_{IIb}\beta_3$ (*28*, *29*). Docking studies, MD simulations, and crystallographic structural data defined its mode of binding, which was further supported by cross-species and mutagenesis studies (*28*, *29*). Here, we have built on these data by rationally designing, synthesizing, and then analyzing the binding of RUC-2, a RUC-1 derivative that is greater than 100 times more potent in inhibiting platelet aggregation.

RUC-2 is somewhat larger than RUC-1 (molecular weight, 385 versus 265) but still well below the 500 molecular weight cutoff commonly used to assess a compound's suitability to function as an oral therapeutic. It retains many of RUC-1's properties, including selectivity for $\alpha_{IIb}\beta_3$ compared to $\alpha_V\beta_3$, and for human $\alpha_{IIb}\beta_3$ compared to mouse or rat $\alpha_{IIb}\beta_3$. It also shares RUC-1's decreased ability to induce the β_3 LIBS epitopes compared to eptifibatide, suggesting that it induces less extensive conformational changes in the receptor. In accord with this hypothesis and in contrast with the results with both eptifibatide and tirofiban, RUC-2 did not induce $\alpha_{IIb}\beta_3$ receptor extension as judged by electron micrographs of $\alpha_{IIb}\beta_3$ inserted into nanodiscs, nor did it produce the major shift in elution volume in gel filtration or the major change in DLS produced by these drugs. Studies by several investigators on different RGD-based $\alpha_{IIb}\beta_3$ antagonists showed that the antagonists that induce exposure of β_3 LIBS epitopes all share a structure that includes a carboxyl capable of coordinating the MIDAS metal ion (*14*, *16*, *37*–*39*). Moreover, unlike eptifibatide and tirofiban, RUC-2 did not "prime" the $\alpha_{IIb}\beta_3$ receptor, that is, induce it to adopt a high-affinity fibrinogen binding conformation (*16*, *20*, *36*, *37*, *40*). This is of particular note because the capacity to prime the receptor may explain the lack of efficacy and variable increase in mortality associated with the first generation of oral $\alpha_{IIb}\beta_3$ antagonists, which were based on the RGD sequence (*11*, *12*, *14*). We used a modification of the original priming assay developed by Du *et al.* (*36*), which uses fixation before washing away the agent. We and others have developed variations of this assay, some of which do not involve fixation (*16*, *28*, *37*, *40*, *41*), and we obtained similar results with RUC-1 using one of these assays (*28*). After evaluating a number of different assays, we found that the assay we used in this study provided the most consistent results. However, none of these assays has been validated with in vivo data.

After ligand binding, integrin receptors are capable of initiating outside-in signaling (*7*). We did not directly study the effect of RUC-2 on such signaling, but because ligand binding is associated with conformational changes in the β_3 subunit (*23*), RUC-2's inability to induce such changes may make it less likely to induce outside-in signaling.

To further explore the conformational changes induced in $\alpha_{IIb}\beta_3$ by RUC-1 and RUC-2, we analyzed the effect of the compounds on

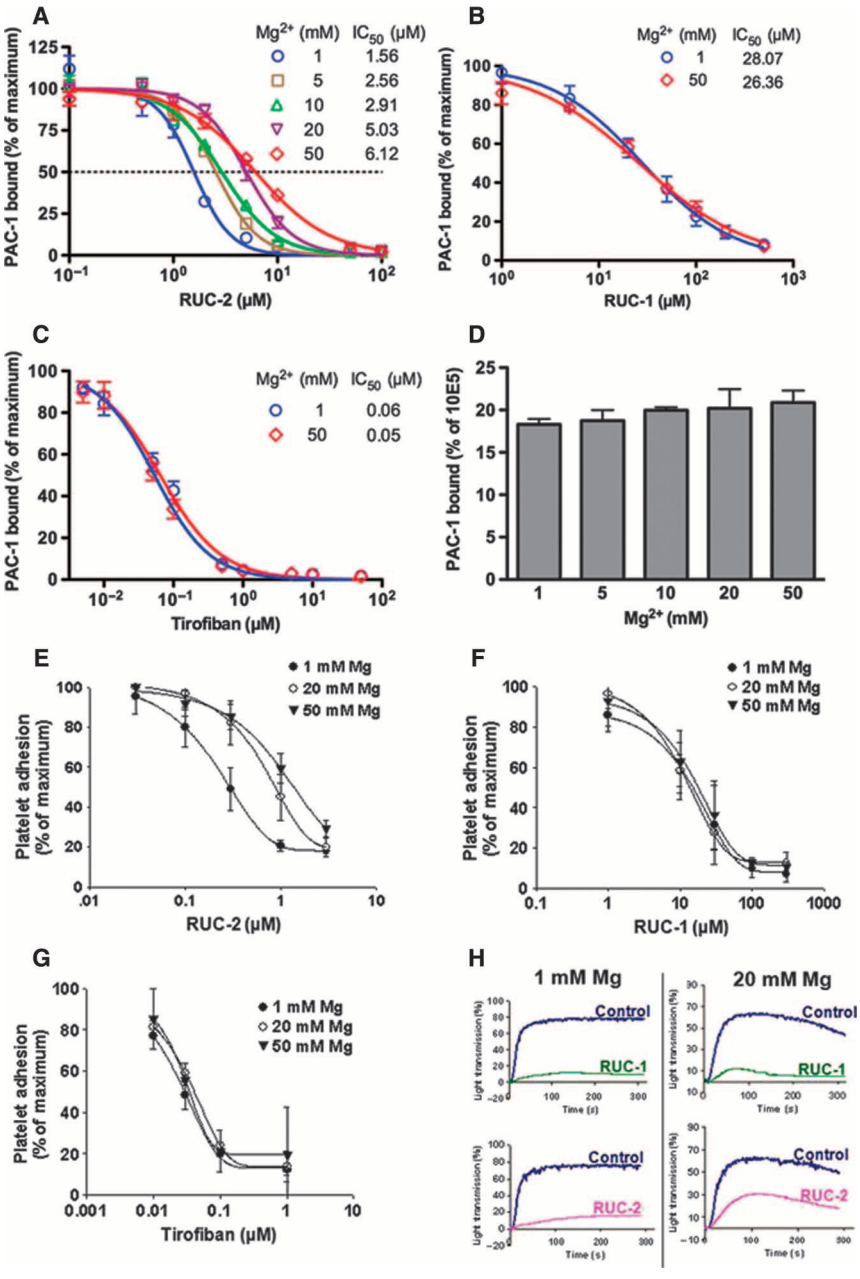

Fig. 6. Effect of Mg^{2+} concentration on RUC-2's ability to inhibit ligand binding to $\alpha_{IIb}\beta_3$. (**A** to **C**) Inhibition of PAC-1 binding to $\alpha_{IIb}\beta_3$ in CHO-K cells in the presence of the activating mAb PT25-2 by RUC-2 (A), RUC-1 (B), or tirofiban (C) at indicated concentrations of Mg^{2+} plus 1 mM Ca^{2+}. Data are means ± SD of percentage of MFI in the presence versus absence of drug (maximum binding) ($n = 3$). (**D**) PAC-1 binding to CHO-K cells expressing $\alpha_{IIb}\beta_3$ in the presence of PT25-2, normalized for $\alpha_{IIb}\beta_3$ expression (mAb 10E5 binding) at indicated concentrations of Mg^{2+} plus 1 mM Ca^{2+} in the absence of drug. PAC-1 binding is the mean ± SD of percentage of MFI of PAC-1 binding to the MFI of 10E5 binding ($n = 3$). (**E** to **G**) Effect of Mg^{2+} concentration on platelet adhesion to fibrinogen in the presence of RUC-2 (E), RUC-1 (F), or tirofiban (G). Washed platelets in buffers containing 1 mM Ca^{2+} plus 1, 20, or 50 mM Mg^{2+} were added to wells precoated with fibrinogen (50 μg/ml) for 60 min at 22°C. After washing, adherent platelets were detected by acid phosphatase activity. Results are expressed as means ± SD ($n = 3$ for RUC-2 and RUC-1; $n = 2$ for tirofiban). (**H**) Effect of Mg^{2+} on platelet aggregation induced by ADP in the presence of RUC-2 (1 μM) or RUC-1 (100 μM). Washed platelets were resuspended in buffer containing fibrinogen (200 μg/ml) and 1 mM Ca^{2+} in combination with either 1 or 20 mM Mg^{2+}. Aggregation was induced by adding a thrombin receptor–activating peptide (SFLLRN) at 10 μM. Results from one of two similar experiments are shown.

inducing platelet recruitment of IgG from the serum of patients who developed thrombocytopenia when treated with either tirofiban or eptifibatide. In these cases, the drug used to treat the patient induced recruitment of IgG to the platelet. In contrast, neither RUC-1 nor RUC-2 induced recruitment of IgG compared to control in all five patients studied with tirofiban-dependent thrombocytopenia. Similarly, in 13 of 15 patients with eptifibatide-dependent thrombocytopenia, neither RUC-1 nor RUC-2 induced IgG recruitment. In one patient with eptifibatide-dependent thrombocytopenia, however, both RUC-1 and RUC-2 enhanced platelet IgG recruitment to a minor degree, and in another, RUC-2, but not RUC-1, induced substantial IgG recruitment. Thus, in most cases, RUC-2 does not expose and/or contribute to the neoepitopes induced and/or created by tirofiban or eptifibatide that are recognized by patient IgG and that are associated with the development of clinical thrombocytopenia. It is possible, however, that RUC-2 can induce platelet recruitment of other individuals' IgG and that this could lead to thrombocytopenia.

To assess the structural basis for RUC-2's greater potency than RUC-1, we used both computational and x-ray crystallographic techniques. By soaking RUC-2 into the closed $\alpha_{IIb}\beta_3$ headpiece crystal in the presence of 1 mM Ca^{2+} and 5 mM Mg^{2+}, we obtained good electron density for RUC-2 at the RGD binding pocket of $\alpha_{IIb}\beta_3$. The RUC-2 crystal structure showed the same α_{IIb} subunit binding features as did RUC-1. In addition, the primary amine of RUC-2 interacted with the β_3 subunit by forming a hydrogen bond to the carboxyl oxygen of Glu^{220} that ordinarily coordinates the MIDAS Mg^{2+}, and RUC-2's phenylacetamide nitrogen formed a hydrogen bond to the backbone oxygen of β_3 Asn^{215}. These additional interactions and the hydrophobic interactions of the phenyl ring of RUC-2 with the β_3 subunit most likely account for its more than 100-fold higher affinity for $\alpha_{IIb}\beta_3$ than RUC-1. Remarkably, no electron density for the Mg^{2+} ion at the MIDAS was visible in the $\alpha_{IIb}\beta_3$ headpiece–RUC-2 complex structure. This is in contrast to our previously reported native crystal structures in the presence of 5 mM Mg^{2+}, which showed clear electron density for the Mg^{2+} ion in the MIDAS (*30*). To assess whether RUC-2 was

competing for binding to the β_3 Glu^{220} MIDAS carboxyl oxygen, we also soaked RUC-2 into the crystal in the presence of 20 mM Mg^{2+}. Both of the two higher-resolution data sets obtained under these conditions showed clear densities for a Mg^{2+} at the MIDAS, but no densities for RUC-2. These results indicate that RUC-2 and the Mg^{2+} ion compete with each other for binding to β_3. In the absence of ligand, the MIDAS Mg^{2+} ion is held in place by direct coordination by one of the side-chain oxygens of Glu^{220} and the side-chain oxygen of Ser^{121}, as well as indirect coordination by Asp^{119} and Ser^{123} through water molecules. The other Glu^{220} carboxyl oxygen directly coordinates the Ca^{2+} in the SyMBS, and thus, it plays a major role in the structures of both the SyMBS and the MIDAS. The importance of the MIDAS metal ion in ligand binding is well established from mutational studies of cells expressing recombinant $\alpha_{IIb}\beta_3$, studies of patients with the hemorrhagic disorder Glanzmann thrombasthenia who harbor naturally occurring mutations (*42*, *43*), and the crystallographic evidence that ligands bind to $\alpha_{IIb}\beta_3$ through direct coordination of the MIDAS Mg^{2+} by a carboxyl oxygen (*22*, *23*). The crystal structure also provides important information on RUC-2's propensity to induce conformational changes in $\alpha_{IIb}\beta_3$. Thus, RUC-2, like RUC-1, does not induce conformational changes in either the α_{IIb} or the β_3 subunits in the $\alpha_{IIb}\beta_3$ headpiece.

The results of molecular docking and MD simulation studies of RUC-2 performed in the absence of the MIDAS Mg^{2+} support the stability of the hydrogen bond between RUC-2's primary amine group and the carboxyl oxygen of Glu^{220} that ordinarily coordinates the MIDAS Mg^{2+} ion. This interaction was observed whether the primary amine was uncharged or positively charged, but the interaction was tighter when the primary amine group of RUC-2 was positively charged. The pK_a (where K_a is the acid dissociation constant) 1 and pK_a 2 values of RUC-2 (corresponding to the primary amine and piperazine nitrogen, respectively) determined directly by titration in water were 6.41 and 8.08, respectively. The value of pK_a 1 is significantly lower than that of primary amines in amino acids (~8.8 to 10.8); however, the functional pK_a value of the primary amine is likely influenced by the binding pocket microenvironment of $\alpha_{IIb}\beta_3$.

A review of the Mg^{2+} concentration data in the crystal structure studies of $\alpha_{IIb}\beta_3$ and $\alpha_V\beta_3$ demonstrates that the MIDAS was not clearly filled with Mg^{2+} in the absence of exogenous Mg^{2+} or in the presence of 1 mM Mg^{2+}, but was filled at concentrations of 5 mM or above (*21*, *23*, *30*, *44*). We could not identify any studies in which the affinity of Mg^{2+} for the $\alpha_{IIb}\beta_3$ MIDAS was directly determined, but Pesho *et al.* (*45*) found that it required millimolar concentrations of Mg^{2+} to displace Ca^{2+} from the MIDAS of an isolated β_3 βI domain containing a mutation in the ADMIDAS (D126A). Our crystal structure data obtained at 5 and 20 mM Mg^{2+} suggest that RUC-2 can compete successfully with Mg^{2+} for binding to Glu^{220} at 5 mM, but not 20 mM. In support of a competition between Mg^{2+} and RUC-2 for binding to β_3, we found that high concentrations of Mg^{2+} increased RUC-2's IC_{50} for inhibiting both ligand binding to recombinant $\alpha_{IIb}\beta_3$ and platelet $\alpha_{IIb}\beta_3$-mediated adhesion to fibrinogen, as well as platelet aggregation induced by a thrombin receptor–activating peptide. In contrast, increasing the Mg^{2+} concentration had little effect on inhibition by tirofiban and/or RUC-1 in the same systems.

RUC-2 may offer advantages over existing intravenous $\alpha_{IIb}\beta_3$ antagonists if its reduced capacity to induce conformational changes in the receptor translates into a reduced incidence of thrombocytopenia and a decreased capacity to paradoxically induce ligand binding. If it is rapidly orally bioavailable or can be modified to become such, it may be especially valuable in the prehospital treatment of myocardial infarction because, currently, more than half of the deaths from myocardial infarction occur during the prehospital phase (~300,000 deaths per year in the United States alone) (*46*), and early treatment with $\alpha_{IIb}\beta_3$ antagonists can increase blood flow, decrease mortality, and even abort the progression of myocardial infarction in more than 25% of cases if administered in the first hour (*25*, *26*, *47*–*49*). Definitive testing of the value of RUC-2 or a related derivative of RUC-2 in the prehospital setting could be performed in a randomized study of ambulance administration of RUC-2 versus placebo; indeed, in a study that enrolled just 179 patients with this trial design, abciximab demonstrated statistically significant benefits in infarct size, left ventricle ejection fraction, major adverse coronary events, ST segment elevation resolution, and heart failure (*50*).

Although RUC-2 is highly specific for human α_{IIb}, preclinical testing can be performed in mice that have targeted deletion of murine α_{IIb} and insertion of human α_{IIb}, as we demonstrated with RUC-1 (*29*). In addition, preclinical testing of RUC-2's effect on the ability of human platelets to form thrombi in vivo can be performed in mice that carry an engineered von Willebrand factor that interacts with human GPIb (*51*). The clinical relevance of this model is supported by the strong correlation between the antithrombotic effects of the currently approved antiplatelet agents in this model and their observed clinical efficacy (*52*).

In conclusion, we report that RUC-2, a high-affinity derivative of RUC-1, specifically inhibits ligand binding by a novel mechanism, leading to loss of the MIDAS metal ion while producing only minor changes in the conformation of β_3. Although there are theoretical reasons to hope that RUC-2 will have therapeutic advantages over existing $\alpha_{IIb}\beta_3$ antagonists, this remains to be tested directly.

MATERIALS AND METHODS

Synthesis of RUC-2

The synthesis of RUC-2 (NCGC00183896-01) is shown in fig. S1 and described in detail in the Supplementary Materials.

Purification of integrin $\alpha_{IIb}\beta_3$

$\alpha_{IIb}\beta_3$ was purified from outdated single-donor platelet concentrates obtained from the New York Blood Center as described in detail in the Supplementary Methods. In brief, washed platelets were lysed in *n*-octyl-β-D-glucoside and $\alpha_{IIb}\beta_3$ was purified by sequential concanavalin A, heparin, Q-Sepharose, and Sephacryl S300 HR chromatography.

Preparation of $\alpha_{IIb}\beta_3$-containing nanodiscs

$\alpha_{IIb}\beta_3$-containing nanodiscs were prepared by a modification of previously described techniques (*35*, *53*, *54*). In brief, a His-tagged membrane scaffold protein was prepared as a recombinant protein in *Escherichia coli*, and final assembly consisted of solubilizing an equimolar mixture of 1,2-dimyristoyl-*sn*-glycero-3-phosphocholine and 1,2-dimyristoyl-*sn*-glycero-3-phospho-(1′-rac-glycerol) in octylglucoside and cholate and then adding the purified $\alpha_{IIb}\beta_3$. The detergents were removed with macroporous polymeric beads (Bio-Bead SM-2), and then the $\alpha_{IIb}\beta_3$ nanodiscs were separated from the empty nanodiscs by gel filtration.

Negative staining EM and evaluation of $\alpha_{IIb}\beta_3$ nanodisc particle size

$\alpha_{IIb}\beta_3$ nanodiscs were treated with eptifibatide, tirofiban, RUC-1, or RUC-2 for 1 hour at room temperature at the concentrations indicated in the text. Samples were loaded onto carbon-coated copper grids that were glow-discharged and then stained with 2% uranyl acetate, followed by drying. Imaging of $\alpha_{IIb}\beta_3$ nanodiscs was performed with a JEOL JEM 100CX transmission electron microscope at 80 kV and magnifications of ×33,000 and ×50,000. The images of $\alpha_{IIb}\beta_3$ nanodiscs were taken from randomly chosen fields on each EM grid. Between 100 and 150 $\alpha_{IIb}\beta_3$ nanodisc particles were present in each image at a magnification of ×33,000. The lengths of all of the particles in each image were measured with ImageJ [National Institutes of Health (NIH)].

Platelet function assays

The following assays were all carried out as previously described (*28*, *30*): platelet and HEK293 cell adhesion to fibrinogen, platelet adhesion/aggregation on collagen, platelet aggregation to ADP (5 μM), binding of fluorescent fibrinogen to platelets in the presence of the activating mAb PT25-2, binding of the α_{IIb}-specific (PMI-1) and β_3-specific (AP5 and LIBS1) LIBS mAbs to platelets, and HEK293 cell $\alpha_V\beta_3$-mediated adhesion to vitronectin.

Priming assay

To assess the ability of eptifibatide, tirofiban, RUC-1, and RUC-2 to induce the high-affinity, ligand-binding state of the $\alpha_{IIb}\beta_3$ receptor, we used a modified version of the assay developed by Du *et al.* (*36*). Platelets washed in Hepes-modified Tyrode's buffer were incubated with the compounds for 20 min at room temperature, fixed with 1% paraformaldehyde for 40 min at room temperature, incubated with 5 mM glycine for 5 min at room temperature, washed four times, resuspended in buffer containing 2 mM Ca^{2+} and 1 mM Mg^{2+}, incubated with Alexa Fluor 488–conjugated fibrinogen (200 μg/ml; Invitrogen) (with or without 10 μM eptifibatide) for 30 min at 37°C, washed, diluted 10-fold, and analyzed by flow cytometry. The net fluorescence was calculated by determining the percentage of platelets with fluorescence values greater than 25 arbitrary units and subtracting the percentage in the untreated samples. In the four experiments, the mean ± SD values in the untreated samples were 9 ± 3%.

Protein expression, purification, and crystallography

The expression, purification, and crystallization of the $\alpha_{IIb}\beta_3$ headpiece (α_{IIb} β-propeller, thigh, and calf-1 domains and β_3 βI, hybrid, PSI, and IEGF-1 domains) in complex with 10E5 Fab were performed as previously described (*30*). RUC-2 was soaked into the $\alpha_{IIb}\beta_3$/Fab crystals at 37.5 μM in the crystallization well solution containing 1 mM Ca^{2+} and 5 mM (or 20 mM) Mg^{2+} for 3 to 5 days. Crystals were harvested in 15% PEG 8000 (polyethylene glycol, molecular weight 8000), 0.2 M ammonium sulfate, 0.1 M tris-HCl (pH 8.9) plus 1 mM Ca^{2+} and 5 mM (or 20 mM) Mg^{2+}; cryoprotected with additional glycerol in 5% increments up to a 20% final concentration; and then flash-frozen in liquid nitrogen. Diffraction data collected at ID-23 of APS were solved by molecular replacement. Final refinement with Phenix used translation-libration-screw and noncrystallographic symmetry analyses.

Gel filtration and DLS

The purified $\alpha_{IIb}\beta_3$ headpiece at 2.0 μM was incubated with RUC-1, RUC-2, or tirofiban at 500, 100, and 56 μM, respectively, at 25°C for 1 hour and subjected to Superdex 200 chromatography in tris-buffered saline plus 1 mM Ca^{2+}/Mg^{2+}. DLS of the purified $\alpha_{IIb}\beta_3$ headpiece alone at 20 μM or after mixing with RUC-1, RUC-2, or tirofiban at 500, 100, and 56 μM, respectively, was measured at 25°C with a Viscotek 802 DLS (Viscotek Corp.) in tris-buffered saline plus 1 mM Ca^{2+}/Mg^{2+}.

Molecular docking

The crystal structure of the $\alpha_{IIb}\beta_3$ headpiece cocrystallized with the inhibitor RUC-1 (*28*–*30*) was used for the docking of RUC-2 [Protein Data Bank (PDB) code 3NIF]. After RUC-1 was removed from the structure, RUC-2 docking was performed in the absence of the MIDAS Mg^{2+} ion. The SyMBS and ADMIDAS Ca^{2+} ions were retained, as were the crystallographic water molecules around the ions and the two water molecules close to Asp^{232}. In the latter case, only the MIDAS Mg^{2+} was removed. Further details are provided in the Supplementary Materials.

MD simulations

The MD simulations of the $\alpha_{IIb}\beta_3$ complex with RUC-2 bound in a similar fashion to RUC-1 were carried out on truncated forms of the protein system (that is, α_{IIb} residues 1 to 452 and β_3 residues 108 to 352) with the Amber10.0 suite of programs. Further details are provided in the Supplementary Materials.

Detection of antibodies from patients with tirofiban- or eptifibatide-induced thrombocytopenia

To assess whether RUC-1 or RUC-2 induces conformational changes in $\alpha_{IIb}\beta_3$ similar to those produced by eptifibatide and tirofiban that result in recruitment of IgG to the platelet surface in patients who develop thrombocytopenia after treatment with one or the other drug, we used the assay described previously (*9*). Further details are provided in the Supplementary Materials.

Effect of Mg^{2+} concentration on RUC-2's ability to inhibit ligand binding to $\alpha_{IIb}\beta_3$

CHO-K cells stably expressing human $\alpha_{IIb}\beta_3$ were incubated with or without drugs at the indicated Mg^{2+} concentrations plus 1 mM Ca^{2+} for 30 min, and then incubated with mAb PAC-1 (5 μg/ml) (ligand-mimetic IgM, selective for the activated conformation of $\alpha_{IIb}\beta_3$) plus activating mAb PT25-2 (5 μg/ml) for another 30 min at 25°C. Cells were washed and incubated with phycoerythrin-labeled goat anti-mouse IgM on ice for 30 min and analyzed by flow cytometry after washing. The expression of $\alpha_{IIb}\beta_3$ was detected with mAb 10E5 and Alexa Fluor 488–labeled goat anti-mouse IgG. PAC-1 binding is presented as mean ± SD of percentage of MFI of PAC-1 binding to the MFI of 10E5 binding.

Titration analysis of RUC-2 in water was performed by Analiza Inc. by retention time analysis using parallel capillary electrophoresis separation.

SUPPLEMENTARY MATERIALS

www.sciencetranslationalmedicine.org/cgi/content/full/4/125/125ra32/DC1

Materials and Methods

Fig. S1. Synthesis of RUC-2 (1) (NCGC00183896-01).

Fig. S2. Effect of RUC-1 and RUC-2 on the aggregation of citrated platelet-rich plasma from mice (A), rat (B), and transgenic mice expressing human α_{IIb} and mouse β_3 (C).

Fig. S3. Effect of mAbs 6F1, 10E5, or 7E3, RUC-1, and RUC-2 on platelet adhesion to collagen.

Fig. S4. Effect of mAbs LM609 or 7E3, RUC-1, and RUC-2 on adhesion of HEK293 cells expressing $\alpha_V\beta_3$ to vitronectin and HEK293 cells expressing $\alpha_{IIb}\beta_3$ to fibrinogen.

Fig. S5. Induction of ligand-induced binding site (LIBS) epitopes.
Fig. S6. Ligand-binding pocket of $\alpha_{IIb}\beta_3$ headpiece crystal soaked with RUC-2 and 20 mM Mg^{2+}.
Fig. S7. Results of the MD simulations of the RUC-2–$\alpha_{IIb}\beta_3$ fragment complexes in the absence of the MIDAS Mg^{2+} ion.
References

REFERENCES AND NOTES

1. R. O. Hynes, Integrins: Bidirectional, allosteric signaling machines. *Cell* **110**, 673–687 (2002).
2. B. H. Luo, C. V. Carman, T. A. Springer, Structural basis of integrin regulation and signaling. *Annu. Rev. Immunol.* **25**, 619–647 (2007).
3. K. Ley, C. Laudanna, M. I. Cybulsky, S. Nourshargh, Getting to the site of inflammation: The leukocyte adhesion cascade updated. *Nat. Rev. Immunol.* **7**, 678–689 (2007).
4. W. Zou, S. L. Teitelbaum, Integrins, growth factors, and the osteoclast cytoskeleton. *Ann. N. Y. Acad. Sci.* **1192**, 27–31 (2010).
5. P. T. Caswell, S. Vadrevu, J. C. Norman, Integrins: Masters and slaves of endocytic transport. *Nat. Rev. Mol. Cell Biol.* **10**, 843–853 (2009).
6. X. Lu, D. Lu, M. Scully, V. Kakkar, The role of integrins in cancer and the development of anti-integrin therapeutic agents for cancer therapy. *Perspect. Medicin. Chem.* **2**, 57–73 (2008).
7. B. S. Coller, S. J. Shattil, The GPIIb/IIIa (integrin αIIbβ3) odyssey: A technology-driven saga of a receptor with twists, turns, and even a bend. *Blood* **112**, 3011–3025 (2008).
8. X. Bosch, J. Marrugat, J. Sanchis, Platelet glycoprotein IIb/IIIa blockers during percutaneous coronary intervention and as the initial medical treatment of non-ST segment elevation acute coronary syndromes. *Cochrane Database Syst. Rev.* **9**, CD002130 (2010).
9. D. W. Bougie, P. R. Wilker, E. D. Wuitschick, B. R. Curtis, M. Malik, S. Levine, R. N. Lind, J. Pereira, R. H. Aster, Acute thrombocytopenia after treatment with tirofiban or eptifibatide is associated with antibodies specific for ligand-occupied GPIIb/IIIa. *Blood* **100**, 2071–2076 (2002).
10. C. Gao, B. Boylan, D. Bougie, J. C. Gill, J. Birenbaum, D. K. Newman, R. H. Aster, P. J. Newman, Eptifibatide-induced thrombocytopenia and thrombosis in humans require FcγRIIa and the integrin β3 cytoplasmic domain. *J. Clin. Invest.* **119**, 504–511 (2009).
11. D. P. Chew, D. L. Bhatt, E. J. Topol, Oral glycoprotein IIb/IIIa inhibitors: Why don't they work? *Am. J. Cardiovasc. Drugs* **1**, 421–428 (2001).
12. D. Cox, Oral GPIIb/IIIa antagonists: What went wrong? *Curr. Pharm. Des.* **10**, 1587–1596 (2004).
13. B. M. Scirica, C. P. Cannon, R. Cooper, R. H. Aster, J. Brassard, C. H. McCabe, A. Charlesworth, A. M. Skene, E. Braunwald, Drug-induced thrombocytopenia and thrombosis: Evidence from patients receiving an oral glycoprotein IIb/IIIa inhibitor in the Orbofiban in Patients with Unstable coronary Syndromes- (OPUS-TIMI 16) trial. *J. Thromb. Thrombolysis* **22**, 95–102 (2006).
14. L. K. Jennings, J. H. Haga, S. M. Slack, Differential expression of a ligand induced binding site (LIBS) by GPIIb-IIIa ligand recognition peptides and parenteral antagonists. *Thromb. Haemost.* **84**, 1095–1102 (2000).
15. W. C. Kouns, D. Kirchhofer, P. Hadváry, A. Edenhofer, T. Weller, G. Pfenninger, H. R. Baumgartner, L. K. Jennings, B. Steiner, Reversible conformational changes induced in glycoprotein IIb-IIIa by a potent and selective peptidomimetic inhibitor. *Blood* **80**, 2539–2547 (1992).
16. K. Peter, M. Schwarz, J. Ylänne, B. Kohler, M. Moser, T. Nordt, P. Salbach, W. Kübler, C. Bode, Induction of fibrinogen binding and platelet aggregation as a potential intrinsic property of various glycoprotein IIb/IIIa ($\alpha_{IIb}\beta_3$) inhibitors. *Blood* **92**, 3240–3249 (1998).
17. S. Epelman, D. Nair, R. Downey, M. Militello, A. T. Askari, Eptifibatide-induced thrombocytopenia and thrombosis. *J. Thromb. Thrombolysis* **22**, 151–154 (2006).
18. D. P. Chew, D. L. Bhatt, S. Sapp, E. J. Topol, Increased mortality with oral platelet glycoprotein IIb/IIIa antagonists: A meta-analysis of phase III multicenter randomized trials. *Circulation* **103**, 201–206 (2001).
19. D. Seiffert, A. M. Stern, W. Ebling, R. J. Rossi, Y. C. Barrett, R. Wynn, G. F. Hollis, B. He, C. J. Kieras, D. L. Pedicord, D. A. Cromley, T. A. Hua, R. B. Stein, R. N. Daly, A. Sferruzza, H. J. Pieniaszek, J. T. Billheimer, Prospective testing for drug-dependent antibodies reduces the incidence of thrombocytopenia observed with the small molecule glycoprotein IIb/IIIa antagonist roxifiban: Implications for the etiology of thrombocytopenia. *Blood* **101**, 58–63 (2003).
20. N. Bassler, C. Loeffler, P. Mangin, Y. Yuan, M. Schwarz, C. E. Hagemeyer, S. U. Eisenhardt, I. Ahrens, C. Bode, S. P. Jackson, K. Peter, A mechanistic model for paradoxical platelet activation by ligand-mimetic $\alpha_{IIb}\beta_3$ (GPIIb/IIIa) antagonists. *Arterioscler. Thromb. Vasc. Biol.* **27**, e9–e15 (2007).
21. J. Zhu, B. H. Luo, T. Xiao, C. Zhang, N. Nishida, T. A. Springer, Structure of a complete integrin ectodomain in a physiologic resting state and activation and deactivation by applied forces. *Mol. Cell* **32**, 849–861 (2008).
22. T. A. Springer, J. Zhu, T. Xiao, Structural basis for distinctive recognition of fibrinogen γC peptide by the platelet integrin $\alpha_{IIb}\beta_3$. *J. Cell Biol.* **182**, 791–800 (2008).
23. T. Xiao, J. Takagi, B. S. Coller, J. H. Wang, T. A. Springer, Structural basis for allostery in integrins and binding to fibrinogen-mimetic therapeutics. *Nature* **432**, 59–67 (2004).
24. J. Takagi, K. Strokovich, T. A. Springer, T. Walz, Structure of integrin $\alpha_5\beta_1$ in complex with fibronectin. *EMBO J.* **22**, 4607–4615 (2003).
25. A. K. Hassan, J. W. Jukema, A. van der Laarse, H. Hasan-Ali, R. Wolterbeek, F. van der Kley, F. Spano, D. E. Atsma, M. J. Schalij, Incidence, patient characteristics and predictors of aborted myocardial infarction in patients undergoing primary PCI: Prospective study comparing pre- and in-hospital abciximab pretreatment. *EuroIntervention* **4**, 662–668 (2009).
26. G. De Luca, C. M. Gibson, F. Bellandi, S. Murphy, M. Maioli, M. Noc, U. Zeymer, D. Dudek, H. R. Arntz, S. Zorman, H. M. Gabriel, A. Emre, D. Cutlip, G. Biondi-Zoccai, T. Rakowski, M. Gyongyosi, P. Marino, K. Huber, A. W. van't Hof, Early glycoprotein IIb–IIIa inhibitors in primary angioplasty (EGYPT) cooperation: An individual patient data meta-analysis. *Heart* **94**, 1548–1558 (2008).
27. G. Montalescot, P. Barragan, O. Wittenberg, P. Ecollan, S. Elhadad, P. Villain, J. M. Boulenc, M. C. Morice, L. Maillard, M. Pansiéri, R. Choussat, P. Pinton; ADMIRAL Investigators. Abciximab before Direct Angioplasty and Stenting in Myocardial Infarction Regarding Acute and Long-Term Follow-up, Platelet glycoprotein IIb/IIIa inhibition with coronary stenting for acute myocardial infarction. *N. Engl. J. Med.* **344**, 1895–1903 (2001).
28. R. Blue, M. Murcia, C. Karan, M. Jirousková, B. S. Coller, Application of high-throughput screening to identify a novel αIIb-specific small-molecule inhibitor of αIIbβ3-mediated platelet interaction with fibrinogen. *Blood* **111**, 1248–1256 (2008).
29. R. Blue, M. A. Kowalska, J. Hirsch, M. Murcia, C. A. Janczak, A. Harrington, M. Jirouskova, J. Li, R. Fuentes, M. A. Thornton, M. Filizola, M. Poncz, B. S. Coller, Structural and therapeutic insights from the species specificity and in vivo antithrombotic activity of a novel αIIb-specific αIIbβ3 antagonist. *Blood* **114**, 195–201 (2009).
30. J. Zhu, J. Zhu, A. Negri, D. Provasi, M. Filizola, B. S. Coller, T. A. Springer, Closed headpiece of integrin $\alpha_{IIb}\beta_3$ and its complex with an $\alpha_{IIb}\beta_3$-specific antagonist that does not induce opening. *Blood* **116**, 5050–5059 (2010).
31. B. S. Coller, J. H. Beer, L. E. Scudder, M. H. Steinberg, Collagen-platelet interactions: Evidence for a direct interaction of collagen with platelet GPIa/IIa and an indirect interaction with platelet GPIIb/IIIa mediated by adhesive proteins. *Blood* **74**, 182–192 (1989).
32. S. Honda, Y. Tomiyama, A. J. Pelletier, D. Annis, Y. Honda, R. Orchekowski, Z. Ruggeri, T. J. Kunicki, Topography of ligand-induced binding sites, including a novel cation-sensitive epitope (AP5) at the amino terminus, of the human integrin β_3 subunit. *J. Biol. Chem.* **270**, 11947–11954 (1995).
33. A. L. Frelinger III, I. Cohen, E. F. Plow, M. A. Smith, J. Roberts, S. C. Lam, M. H. Ginsberg, Selective inhibition of integrin function by antibodies specific for ligand-occupied receptor conformers. *J. Biol. Chem.* **265**, 6346–6352 (1990).
34. P. J. Shadle, M. H. Ginsberg, E. F. Plow, S. H. Barondes, Platelet-collagen adhesion: Inhibition by a monoclonal antibody that binds glycoprotein IIb. *J. Cell Biol.* **99**, 2056–2060 (1984).
35. F. Ye, G. Hu, D. Taylor, B. Ratnikov, A. A. Bobkov, M. A. McLean, S. G. Sligar, K. A. Taylor, M. H. Ginsberg, Recreation of the terminal events in physiological integrin activation. *J. Cell Biol.* **188**, 157–173 (2010).
36. X. P. Du, E. F. Plow, AL Frelinger III, T. E. O'Toole, J. C. Loftus, M. H. Ginsberg, Ligands "activate" integrin $\alpha_{IIb}\beta_3$ (platelet GPIIb-IIIa). *Cell* **65**, 409–416 (1991).
37. R. R. Hantgan, M. C. Stahle, Integrin priming dynamics: Mechanisms of integrin antagonist-promoted αIIbβ3:PAC-1 molecular recognition. *Biochemistry* **48**, 8355–8365 (2009).
38. R. R. Hantgan, M. C. Stahle, J. H. Connor, R. F. Connor, S. A. Mousa, $\alpha_{IIb}\beta_3$ priming and clustering by orally active and intravenous integrin antagonists. *J. Thromb. Haemost.* **5**, 542–550 (2007).
39. S. Honda, Y. Tomiyama, T. Aoki, M. Shiraga, Y. Kurata, J. Seki, Y. Matsuzawa, Association between ligand-induced conformational changes of integrin $\alpha_{IIb}\beta_3$ and $\alpha_{IIb}\beta_3$-mediated intracellular Ca^{2+} signaling. *Blood* **92**, 3675–3683 (1998).
40. R. R. Hantgan, M. C. Stahle, S. T. Lord, Dynamic regulation of fibrinogen: Integrin αIIbβ3 binding. *Biochemistry* **49**, 9217–9225 (2010).
41. A. L. Frelinger III, M. I. Furman, L. A. Krueger, M. R. Barnard, A. D. Michelson, Dissociation of glycoprotein IIb/IIIa antagonists from platelets does not result in fibrinogen binding or platelet aggregation. *Circulation* **104**, 1374–1379 (2001).
42. E. K. Baker, E. C. Tozer, M. Pfaff, S. J. Shattil, J. C. Loftus, M. H. Ginsberg, A genetic analysis of integrin function: Glanzmann thrombasthenia in vitro. *Proc. Natl. Acad. Sci. U.S.A.* **94**, 1973–1978 (1997).
43. J. C. Loftus, T. E. O'Toole, E. F. Plow, A. Glass, A. L. Frelinger III, M. H. Ginsberg, A β_3 integrin mutation abolishes ligand binding and alters divalent cation-dependent conformation. *Science* **249**, 915–918 (1990).
44. J. P. Xiong, T. Stehle, B. Diefenbach, R. Zhang, R. Dunker, D. L. Scott, A. Joachimiak, S. L. Goodman, M. A. Arnaout, Crystal structure of the extracellular segment of integrin αVβ3. *Science* **294**, 339–345 (2001).

45. M. M. Pesho, K. Bledzka, L. Michalec, C. S. Cierniewski, E. F. Plow, The specificity and function of the metal-binding sites in the integrin β_3 A-domain. *J. Biol. Chem.* **281**, 23034–23041 (2006).
46. V. L. Roger, A. S. Go, D. M. Lloyd-Jones, R. J. Adams, J. D. Berry, T. M. Brown, M. R. Carnethon, S. Dai, G. de Simone, E. S. Ford, C. S. Fox, H. J. Fullerton, C. Gillespie, K. J. Greenlund, S. M. Hailpern, J. A. Heit, P. M. Ho, V. J. Howard, B. M. Kissela, S. J. Kittner, D. T. Lackland, J. H. Lichtman, L. D. Lisabeth, D. M. Makuc, G. M. Marcus, A. Marelli, D. B. Matchar, M. M. McDermott, J. B. Meigs, C. S. Moy, D. Mozaffarian, M. E. Mussolino, G. Nichol, N. P. Paynter, W. D. Rosamond, P. D. Sorlie, R. S. Stafford, T. N. Turan, M. B. Turner, N. D. Wong, J. Wylie-Rosett; American Heart Association Statistics Committee and Stroke Statistics Subcommittee, Heart disease and stroke statistics—2011 update: A report from the American Heart Association. *Circulation* **123**, e18–e209 (2011).
47. H. K. Gold, H. D. Garabedian, R. E. Dinsmore, L. J. Guerrero, J. E. Cigarroa, I. F. Palacios, R. C. Leinbach, Restoration of coronary flow in myocardial infarction by intravenous chimeric 7E3 antibody without exogenous plasminogen activators. Observations in animals and humans. *Circulation* **95**, 1755–1759 (1997).
48. Z. Siudak, T. Rakowski, A. Dziewierz, M. Janzon, R. Birkemeyer, J. Stefaniak, Ł. Partyka, K. Zmudka, D. Dudek, Early abciximab use in ST-elevation myocardial infarction treated with primary percutaneous coronary intervention improves long-term outcome. Data from EUROTRANSFER Registry. *Kardiol. Pol.* **68**, 539–543 (2010).
49. G. De Luca, Glycoprotein IIb-IIIa inhibitors. *Cardiovasc. Ther.* 10.1111/j.1755-5922.2011.00293.x (2011).
50. A. K. Hassan, S. S. Liem, F. van der Kley, S. C. Bergheanu, R. Wolterbeek, J. Bosch, M. Bootsma, K. Zeppenfeld, A. van der Laarse, D. E. Atsma, J. W. Jukema, M. J. Schalij, In-ambulance abciximab administration in STEMI patients prior to primary PCI is associated with smaller infarct size, improved LV function and lower incidence of heart failure: Results from the Leiden MISSION! acute myocardial infarction treatment optimization program. *Catheter Cardiovasc. Interv.* **74**, 335–343 (2009).
51. J. Chen, K. Tan, H. Zhou, H. F. Lo, D. T. Roux, R. C. Liddington, T. G. Diacovo, Modifying murine von Willebrand factor A1 domain for in vivo assessment of human platelet therapies. *Nat. Biotechnol.* **26**, 114–119 (2008).
52. J. Magallon, J. Chen, L. Rabbani, G. Dangas, J. Yang, J. Bussel, T. Diacovo, Humanized mouse model of thrombosis is predictive of the clinical efficacy of antiplatelet agents. *Circulation* **123**, 319–326 (2011).
53. T. K. Ritchie, Y. V. Grinkova, T. H. Bayburt, I. G. Denisov, J. K. Zolnerciks, W. M. Atkins, S. G. Sligar, Chapter 11—Reconstitution of membrane proteins in phospholipid bilayer nanodiscs. *Methods Enzymol.* **464**, 211–231 (2009).
54. T. H. Bayburt, S. G. Sligar, Membrane protein assembly into nanodiscs. *FEBS Lett.* **584**, 1721–1727 (2010).

Acknowledgments: We thank S. Rivera for administrative assistance and T. Song and M. Suarez-Farinas for biostatistical support. **Funding:** Supported, in part, by grants HL19278, HL13629, and HL48675 from the National Heart, Lung, and Blood Institute; Clinical and Translational Science Award grant ULRR024143 from the National Center for Research Resources, NIH; the Molecular Libraries Initiative of the NIH Roadmap for Medical Research and the Intramural Research Program of the National Human Genome Research Institute; funds from Stony Brook University; and the National Research Foundation of Korea Grant funded by the Korean Government (NRF-2009-352-E00042). The computations were supported in part by the NSF through TeraGrid advanced computing resources provided by Texas Advanced Computing Center under grant TG-MCB080109N (principal investigator: M.F.). **Author contributions:** Jieqing Zhu designed, performed, and interpreted the crystallography, Stokes radius, and RUC-2–Mg^{2+} competition studies; W.-S.C. designed, performed, and interpreted the nanodisc studies; J.G.M. designed and performed the syntheses of RUC-1 and RUC-2 along with M.S. and W.H.; A.N. designed, performed, and analyzed the MD simulations and docking studies; Jianghai Zhu collected the x-ray diffraction data and refined and interpreted the crystal structures; S.N. and J.L. performed and interpreted the platelet function studies; D.B. designed, conducted, and interpreted the platelet antibody recruitment studies along with M.R.; R.A. designed, oversaw, and interpreted the platelet antibody recruitment studies; C.J.T. designed, oversaw, and interpreted the synthesis studies; M.F. designed, oversaw, and interpreted the MD simulations and docking studies; T.A.S. designed, oversaw, and interpreted the crystallography and Stokes radius studies; and B.S.C. designed, oversaw, and interpreted the platelet function studies. B.S.C. had primary responsibility for writing the manuscript with contributions from W.-S.C., J.G.M., A.N., J.Z., D.B., R.A., C.J.T., M.F., and T.A.S. **Competing interests:** B.S.C. is an inventor of abciximab (Centocor) and, in accord with Federal law and the policies of the Research Foundation of the State University of New York, receives royalties based on the sales of abciximab. He is also an inventor of the VerifyNow assays (Accumetrics) and, in accord with Federal law and the policies of the Mount Sinai School of Medicine, receives royalties based on the sales of the VerifyNow assays. Rockefeller University has applied for patents on RUC-1 and RUC-2. **Data and materials availability:** The structural data have been deposited at the Protein Database (PDB code 3T3M). RUC-2 is available from the authors (B.S.C. and C.J.T.).

Submitted 7 December 2011
Accepted 23 January 2012
Published 14 March 2012
10.1126/scitranslmed.3003576

Citation: J. Zhu, W.-S. Choi, J. G. McCoy, A. Negri, J. Zhu, S. Naini, J. Li, M. Shen, W. Huang, D. Bougie, M. Rasmussen, R. Aster, C. J. Thomas, M. Filizola, T. A. Springer, B. S. Coller, Structure-guided design of a high-affinity platelet integrin $\alpha_{IIb}\beta_3$ receptor antagonist that disrupts Mg^{2+} binding to the MIDAS. *Sci. Transl. Med.* **4**, 125ra32 (2012).

www.sciencetranslationalmedicine.org/cgi/content/full/4/125/125ra32/DC1

Supplementary Materials for

Structure-Guided Design of a High-Affinity Platelet Integrin $\alpha_{IIb}\beta_3$ Receptor Antagonist That Disrupts Mg^{2+} Binding to the MIDAS

Jieqing Zhu, Won-Seok Choi, Joshua G. McCoy, Ana Negri, Jianghai Zhu, Sarasija Naini, Jihong Li, Min Shen, Wenwei Huang, Daniel Bougie, Mark Rasmussen, Richard Aster, Craig J. Thomas, Marta Filizola, Timothy A. Springer, Barry S. Coller*

*To whom correspondence should be addressed. E-mail: collerb@rockefeller.edu

Published 14 March 2012, *Sci. Transl. Med.* **4**, 125ra32 (2012)
DOI: 10.1126/scitranslmed.3003576

The PDF file includes:

Structure-Guided Design of a High Affinity Platelet Integrin αIIbβ3 Receptor Antagonist That Displaces Mg^{2+} from the β3 MIDAS

Supplementary Materials and Methods

Materials: RUC-1, the inactive piperidine derivative of RUC-1, mAbs AP5 (a generous gift of Dr. Peter Newman, BloodCenter of Wisconsin), 10E3, and 7E3, tirofiban, and eptifibatide were obtained as previously described. The αIIbβ3 activating mAb PT25-2 was a generous gift of Dr. Makoto Handa of Keio University, Tokyo, Japan (*1*). n-octyl-β-D-glucoside (OG), 1,2-dimyristoyl-sn-glycero-3-phosphocholine (DMPC), and 1,2-dimyristoyl-sn-glycero-3-phospho-(1'-rac-glycerol) (DMPG) were purchased from Anatrace (Maumee, OH). Prostaglandin E_1 (PGE_1), isopropyl β-D-1-thiogalactopyranoside, α-methyl glucoside, leupeptin, uranyl acetate, and Triton X-100 were purchased from Sigma (St. Louis, MO, USA). Con A-Sepharose, Q-Sepharose, Nickel-Sepharose, Sephacryl S300, Superdex 200HR, and NHS-activated Sepharose were purchased from GE Healthcare (Piscataway, NJ). Bio-Bead SM-2 was purchased from Bio-Rad (Hercules, CA). PAC-1 was purchased from BD Biosciences (San Diego, CA) and 400 mesh carbon-coated copper grids were purchased from Electron Microscopy Sciences (Hatfield, PA).

General Synthetic Methods: Samples were analyzed for purity on an Agilent 1200 series LC/MS using a Zorbax Eclipse XBD-C8 reverse phase (5 micron, 4.6 x 150mm) column and a 1.1 mL/min flow rate. A gradient was performed using an acetonitrile/water mobile phase (each containing 0.1% trifluoroacetic acid). The gradient was 4% to 100% acetonitrile over 7 minutes and purity of final compounds was determined using a two microliter injection with quantitation by AUC at 220 and 254 nanometers. Chromatography on silica gel was performed

using forced flow (liquid) of the indicated solvent system on Biotage KP-Sil prepacked cartridges and using the Biotage SP-1 automated chromatography system. ^{1}H-spectra were recorded on a Varian Inova 400 MHz spectrometer. Chemical shifts are reported in ppm with the solvent resonance as the internal standard ($CDCl_3$ 7.26 ppm and DMSO-d_6 2.5 ppm). High resolution mass spectral data was collected in-house using an Agilent 6210 time-of-flight mass spectrometer, also coupled to an Agilent Technologies 1200 series HPLC system.

Synthesis of RUC-2: To a solution of 5-(3-nitrophenyl)-1,3,4-thiadiazol-2-amine (**2**) (3.0 g, 13.50 mmol) in MeCN (120 mL) was added methyl 3-chloro-3-oxopropanoate (1.735 mL, 16.20 mmol). The mixture was stirred at room temperature for 2 h. After consumption of the starting material, $POCl_3$ (60 mL, 644 mmol) was added along with DIPEA (2.358 mL, 13.50 mmol) in MeCN (10 mL). The mixture was heated in the microwave at 150 °C for 25 min, cooled, and concentrated *in vacuo.* The resulting slurry was taken up in chloroform, poured over ice and washed with saturated $NaHCO_3$, water and brine, dried over $MgSO_4$, and concentrated *in vacuo* to give a dark red oil which was purified via column chromatography on a 100 g snap column with 0-10% EtOAc/DCM gradient elution to give 7-chloro-2-(3-nitrophenyl)-5H-[1,3,4]thiadiazolo[3,2-a]pyrimidin-5-one (**3**) (1.36 g, 4.41 mmol, 32.6 % yield) as an orange solid. To a solution of 7-chloro-2-(3-nitrophenyl)-5H-[1,3,4]thiadiazolo[3,2-a]pyrimidin-5-one (**3**) (1.0 g, 3.24 mmol) in MeCN (30 ml) in a microwave vial was added *tert*-butyl 1-piperazinecarboxylate (0.724 g, 3.89 mmol) followed by DIPEA (1.697 ml, 9.72 mmol). The mixture was heated in the microwave at 150 °C for 25 min., cooled and concentrated *in vacuo* and purified via column chromatography on a 50 g snap column with 0-10% MeOH/DCM gradient elution to give tert-butyl 4-(2-(3-nitrophenyl)-5-oxo-5H-[1,3,4]thiadiazolo[3,2-a]pyrimidin-7-yl)piperazine-1-carboxylate (**4**) (1.44 g, 3.14 mmol, 97 % yield) as a tan solid. To

a solution of tert-butyl 4-(2-(3-nitrophenyl)-5-oxo-5H-[1,3,4]thiadiazolo[3,2-a]pyrimidin-7-yl)piperazine-1-carboxylate (**4**) (769 mg, 1.677 mmol) in EtOH (12 ml) at room temperature was added Raney(R) 2400 nickel (98 mg, 1.677 mmol) followed by hydrazine (0.526 ml, 16.77 mmol) dropwise. The mixture was stirred at room temperature for 4 hours. The reaction was monitored by TLC and LC/MS and additional nickel and hydrazine were added until the starting material disappeared. The mixture was filtered over celite and concentrated *in vacuo* to give crude tert-butyl 4-(2-(3-aminophenyl)-5-oxo-5H-[1,3,4]thiadiazolo[3,2-a]pyrimidin-7-yl)piperazine-1-carboxylate (**5**) (443 mg, 1.034 mmol, 61.6 % yield) as a tan solid. Crude tert-butyl 4-(2-(3-aminophenyl)-5-oxo-5H-[1,3,4]thiadiazolo[3,2-a]pyrimidin-7-yl)piperazine-1-carboxylate (**5**) (60 mg, 0.140 mmol) was dissolved in DMF (1.5 mL). To this solution was added the Boc-glycine (37 mg, 0.210 mmol) then EDC (40.3 mg, 0.210 mmol). After stirring at room temperature for 24 hours, the mixture was taken up in water and ethyl acetate. The layers were separated and the aqueous layer was extracted with ethyl acetate. The combined organic extracts were then washed with water twice, then brine, dried over $MgSO_4$, and concentrated *in vacuo* to give a yellow solid which was purified via column chromatography with 2-7% MeOH/DCM gradient to give tert-butyl 4-(2-(3-(2-(tert-butoxycarbonylamino)acetamido)phenyl)-5-oxo-5H-[1,3,4]thiadiazolo[3,2-a]pyrimidin-7-yl)piperazine-1-carboxylate (crude material confirmed by LCMS analysis). The residue was dissolved in 2 mL of dichloromethane. To this solution trifluoroacetic acid (1 ml, 13.0 mmol) was added and the mixture was stirred for 18 hours. The solution was then concentrated *in vacuo* and washed with dichloromethane to give a crude yellow solid that was dissolved in methanol and purified by preparative HPLC to give 2-amino-N-(3-(5-oxo-7-(piperazin-1-yl)-5H-[1,3,4]thiadiazolo[3,2-a]pyrimidin-2-yl)phenyl)acetamide (RUC-2)(NCGC00183896-01)(**1**) (40

mg, 49%) as a tan solid after HPLC purification. ^{1}H NMR (400 MHz, DMSO-d_6) δ ppm 8.31 (s, 1 H), 7.86 (d, *J*=7.43 Hz, 1 H), 7.48 - 7.58 (m, 2 H), 5.38 (s, 1 H), 3.46 (br. s., 4 H), 3.29 (s, 2 H), 2.67 - 2.76 (m, 4 H); LCMS (electrospray), *m/z* 386.1 $(MH)^+$; HPLC: t_R = 2.70 min, UV_{254} = >95%. HRMS (ESI): *m/z* calcd for $C_{17}H_{20}N_7O_2S$ $[M+H]^+$ 386.1394, found 386.1393. RUC-2 was synthesized as both the free base and a trifluoroacetic acid salt. The free base was soluble in water at concentrations up to 90 μM and in 10% DMSO in water at concentrations up to 1 mM.

Purification of integrin αIIβ3: αIIbβ3 was purified from outdated single donor platelet concentrates obtained from the New York Blood Center by washing platelets in the presence of PGE_1; removing contaminating blood cells by centrifugation; lysing the resuspended platelets at 4^oC in 5% (w/v) n-octyl-β-D-glucoside (OG) in 150 mM NaCl, 20 mM HEPES, 1 mM $CaCl_2$, 1 mM $MgCl_2$, 10 μM leupeptin, pH 7.4; performing concanavalin A affinity chromatography [binding buffer: 150 mM NaCl, 1% (w/v) OG, 20 mM HEPES, 1 mM $CaCl_2$, 1 mM $MgCl_2$, pH 7.4; washing buffer: binding buffer + 20 mM α-methyl glucoside; elution buffer: binding buffer + 1M α-methyl glucoside]; performing heparin affinity chromatography; applying the flow through fraction to Q-Sepharose [binding buffer: 75 mM NaCl, 1% (w/v) OG, 10 mM HEPES, 1 mM $CaCl_2$, 1 mM $MgCl_2$, pH 7.4; washing buffer: binding buffer + 200 mM NaCl; elution buffer: binding buffer + 400 mM NaCl]; and performing gel size exclusion chromatography on Sephacryl S300 HR [running buffer: 150 mM NaCl, 1% (w/v) OG, 10 mM HEPES, 1 mM $CaCl_2$, 1 mM $MgCl_2$, pH 7.4].

Preparation of αIIbβ3-containing nanodiscs: αIIbβ3-containing nanodiscs were prepared by a modification of the techniques described by Ritchie et al., Babyurt and Sligar, and Ye et al. (*2-4*). A full description is being reported separately. In brief, the His-tagged membrane scaffold protein was prepared as a recombinant protein in E. coli and purified by Ni affinity

chromatography and anion exchange chromatography. Final assembly consisted of solubilizing an equimolar mixture of 1,2-dimyristoyl-sn-glycero-3-phosphocholine and 1,2-dimyristoyl-sn-glycero-3-phospho-(1'-rac-glycerol) in octylglucoside and cholate and then adding the purified αIIbβ3. The detergents were removed with macroporous polymeric beads (Bio-Bead SM-2) and then the αIIbβ3 nanodiscs were separated from the empty nanodiscs by gel filtration.

Negative staining electron microscopy and evaluation of αIIbβ3 nanodisc particle size: αIIbβ3 nanodiscs were treated with eptifibatide, tirofiban, RUC-1, or RUC-2 for 1 hour at room temperature at the concentrations indicated in the text. Samples were loaded onto carbon-coated copper grids that were glow-discharged by a carbon coating unit (Edwards; Crowley, UK) and then stained with 2% uranyl acetate, followed by drying. Imaging of αIIbβ3 nanodiscs was performed using a JEOL JEM 100CX transmission electron microscope (Jeol Ltd; Tokyo, Japan) at 80 kV and magnifications of 33,000X and 50,000X. Individual nanodiscs containing αIIbβ3 were manually selected for analysis using Image J (NIH, Bethesda, MD). The distance from the bottom of the nanodisc to the height of the αIIbβ3 complex (nanodisc-integrin length; NIL) was measured as an indicator of integrin extension. The frequency distribution of NIL values was then analyzed for untreated αIIbβ3 nanodiscs and αIIbβ3 nanodiscs in the presence of different compounds.

Platelet function assays: The following assays were all carried out as previously described (*5*, *6*): platelet and HEK293 cell adhesion to fibrinogen; platelet adhesion/aggregation on collagen; platelet aggregation to ADP (5 μM); binding of fluorescent fibrinogen to platelets in the presence of the activating mAb PT25-2; binding of the αIIb-specific (PMI-1) and β3-specific (AP5 and LIBS1) LIBS mAbs to platelets; HEK293 cell αVβ3-mediated adhesion to vitronectin; and Stokes radius determination by chromatography and dynamic light scattering.

Protein expression, purification and crystallography: The expression, purification, and crystallization of the αIIbβ3 headpiece (αIIb β-propeller, thigh, and calf-1 domains and β3 β1, hybrid, PSI, and IEGF-1 domains) in complex with 10E5 Fab were performed as previously described (*6*). RUC-2 was soaked into the αIIbβ3/Fab crystals at 37.5 μM in the crystallization well solution containing 1 mM Ca^{2+} and 5 mM (or 20 mM) Mg^{2+} for 3-5 days. Crystals were harvested in 15% PEG 8000, 0.2 M ammonium sulfate, 0.1 M Tris-HCl, pH 8.9 plus 1 mM Ca^{2+} and 5 mM (or 20 mM) Mg^{2+} and cryoprotected with additional glycerol in 5% increments up to a 20% final concentration, and then flash frozen in liquid nitrogen. Diffraction data collected at ID-23 of APS was solved using molecular replacement. Final refinement with Phenix utilized translation-libration-screw (TLS) and noncrystallographic symmetry (NCS) analyses.

Gel filtration and dynamic light scattering (DLS): The purified $\alpha_{IIb}\beta_3$ headpiece at 2.0 μM was incubated with RUC-1, RUC-2, or tirofiban at 500 μM, 100 μM, and 56 μM, respectively, at 25ºC for 1h and subjected to Superdex 200 chromatography in Tris-buffered saline plus 1 mM Ca^{2+}/Mg^{2+}. DLS of the purified $\alpha_{IIb}\beta_3$ headpiece alone at 20 μM or after mixing with RUC-1, RUC-2, or tirofiban at 500 μM , 100 μM, and 56 μM, respectively, were measured at 25ºC using a Viscotek 802 DLS (Viscotek Corporation) in Tris-buffered saline plus 1 mM Ca^{2+}/Mg^{2+}.

Molecular docking: The crystal structure of the αIIbβ3 headpiece co-crystallized with the inhibitor RUC-1 (*5-7*) was used for the docking of RUC-2 (PDB code 3NIF). After RUC-1 was removed from the structure, RUC-2 docking was performed in the absence of the MIDAS Mg^{2+} ion. The SyMBS and ADMIDAS Ca^{2+} metal ions were retained, as were the crystallographic waters around the ions and the two water molecules close to Asp232. In the latter case, only the MIDAS Mg^{2+} was removed.

Prior to RUC-2 docking, a thorough exploration of the conformational space accessible to the ligand was performed. Specifically, about 3,000 conformations of RUC-2 were obtained using the program OMEGA version 2.3.2 (OpenEye Scientific Software, Santa Fe, NM). The semi-empirical quantum chemistry program AMSOL version 7.0 (Department of Chemistry and Supercomputing, University of Minnesota, Minneapolis, MN) was used to calculate partial atomic charges and transfer free energies.

Docking calculations of RUC-2, with its primary amine either uncharged or positively charged were performed with DOCK 3.5.54 (*8, 9*). Forty-five matching spheres, labeled for chemical matching based on the local receptor environment, were used to replace the atoms of the crystallographic ligand RUC-1. An energy-based score corresponding to the sum of the receptor-ligand electrostatic and van der Waals interaction energies corrected for ligand desolvation were assigned to each conformation. The best scored conformations of RUC-2 maintaining the same stable interactions of RUC-1(*6*) within the αIIbβ3 binding site received 100 steps of rigid-body energy minimization prior to further optimization using standard molecular dynamics (MD) simulations.

Molecular Dynamics (MD) simulations: The MD simulations of the selected complexes of αIIbβ3 with RUC-2 bound in a similar fashion to RUC-1 were carried out on truncated forms of the protein system (i.e., αIIb residues 1-452 and β3 residues 108-352) using the AMBER10.0 suite of programs (http://ambermd.org/). The initial geometry of RUC-2 was optimized *ab initio* using a restricted Hartree-Fock (RHF) method and a 6-31G (d) basis set, as implemented in the Gaussian 03 program (*10*), and previously calculated RESP point charges (*5*, *6*). The bonded and non-bonded RUC-2 parameters were automatically assigned using the general AMBER force field (GAFF) for organic molecules (*11*). Each molecular system was neutralized by the addition

of seven or five sodium ions (*12*), and immersed in a rectangular box of ~22,500 TIP3P water molecules. Periodic boundary conditions and the NPT ensemble (constant pressure and temperature) were applied during the MD simulations. Electrostatic interactions were treated using the smooth Particle Mesh Ewald (PME) method (*13*) with a grid spacing of 1 Å. The cutoff distance for the nonbonded interactions was set to 9 Å. The SHAKE algorithm (*14*) was applied to all bonds, and an integration step of 2.0 fs was used. Solvent molecules and counterions were first relaxed by energy minimization and then allowed to redistribute around positionally restrained protein–ligand complexes (25 kcal mol^{-1} $Å^{-2}$) during 0.1 ns. The initial positional restraints were increasingly reduced in a series of four relaxation runs of 0.1 ns each until they were completely removed. The resulting systems were allowed to equilibrate in the absence of any restraints for 10 ns during which system coordinates were collected every 2 ps for further analysis, as previously described (*6*). The molecular visualization package PyMOL was used to visually inspect representative snapshots.

Detection of antibodies from patients with tirofiban- or eptifibatide-induced thrombocytopenia: To assess whether RUC-1 or RUC-2 induce conformational changes in αIIbβ3 similar to those produced by eptifibatide and tirofiban that result in recruitment of IgG to the platelet surface in patients who develop thrombocytopenia after treatment with one or the other drug, we used the assay described previously (*15*). In brief, 10 µl of patient serum diluted 1:5 was incubated with $5x10^6$ washed group O platelets (isolated from citrated whole blood and washed in the presence of PGE_1) together with tirofiban (4 µM), eptifibatide (2.4 µM), RUC-1 (100 µM), or RUC-2 (3.9 µM) in a total volume of 50 µl. After 1 hour at RT, platelets were washed twice in HEPES buffer containing the drug at the same concentration as in the primary mixture and suspended in 25 µl of HEPES buffer containing the drug at twice the concentration

used in the primary mixture and 25 µl of fluorescein-labeled anti-Ig antibody (heavy and light chain-specific), diluted 1:100. After incubation in the dark for 45 minutes, an aliquot was diluted in 0.1 ml buffer and platelet-bound fluorescence was analyzed by flow cytometry (FACScan, Becton-Dickinson). A "positive" reaction was defined as a median platelet fluorescence intensity (MFI) at least twice that of platelets treated identically in the absence of drug. This value always exceeded the value obtained with normal serum plus drug or patient serum in the absence of drug by at least three standard deviations.

Statistical analysis. Data are presented as mean ± SD. Group comparisons were performed by Student's t test. IC_{50} values for platelet aggregation data, which were expressed as a percentage of the control value in the absence of αIIbβ3 antagonist, were estimated from a two-parameter logistic function. The IC_{50} (e) was given by the logistic function:

$$f(x) = \frac{100}{1 + e^{b[log(x) - log(e)]}}$$

where b represents the slope. The drc (dose response curves) package from R open source software (www.R-project.org) was used to compute the IC_{50}s.

Supplementary Figure Legends

Fig. S1. Synthesis of RUC-2 (1) (NCGC00183896-01).

Fig. S2. Effect of RUC-1 and RUC-2 on the aggregation of citrated platelet-rich plasma from mice (**A**), rat (**B**), and transgenic mice expressing human α_{IIb} and mouse β_3 (**C**). RUC-1 was tested at 100 μM and RUC-2 at 1 μM. Aggregation was induced by ADP (30 μM for mouse and rat; 5 μM for human) in the absence of either compound (control) or in the presence of one or the other compound. Single representative tracings are presented.

Fig. S3. Effect of mAbs 6F1, 10E5, or 7E3, RUC-1, and RUC-2 on platelet adhesion to collagen. Rat skin type 1 collagen was immobilized on microtiter plates and washed platelets in buffer containing Mg^{2+} were allowed to adhere for 1 hour in the absence or presence of the mAbs 6F1, 10E5 or 7E3, RUC-1, RUC-2, or RUC-2 + 10E5 at the indicated concentrations.

Fig. S4. Effect of mAbs LM609 or 7E3, RUC-1, and RUC-2 on adhesion of HEK293 cells expressing $\alpha_V\beta_3$ to vitronectin and HEK293 cells expressing $\alpha_{IIb}\beta_3$ to fibrinogen. Cells expressing $\alpha_V\beta_3$ or $\alpha_{IIb}\beta_3$, respectively, were added to microtiter wells precoated with either vitronectin (5 μg/ml) or fibrinogen (50 μg/ml). After 1 hour, the wells were washed and cell adhesion measured by assaying endogenous acid phosphatase activity. mAb LM609 is specific for $\alpha_V\beta_3$ whereas mAb 7E3 reacts with both $\alpha_V\beta_3$ and $\alpha_{IIb}\beta_3$.

Fig. S5. Induction of ligand-induced binding site (LIBS) epitopes. The binding of the β3 antibodies AP5 and LIBS and the LIBS antibody PMI-1 were tested in the presence of eptifibatide (1 μM), RUC-1 (100 μM), and RUC-2 (1 μM). The net fluorescence intensity after

subtracting background binding was expressed as a percentage of the value in the presence of eptifibatide, the positive control.

Fig. S6. Ligand-binding pocket of $\alpha_{IIb}\beta_3$ headpiece crystal soaked with RUC-2 and 20 mM Mg^{2+}. (**A**) Molecule 1 of asymmetric unit. (**B**) Molecule 2 of asymmetric unit. 2Fo-Fc maps at 1.0 σ for water (red spheres), Cl^- ions (green spheres), Ca^{2+} ions (yellow sphere), and Mg^{2+} ion (silver sphere) are shown in blue. Selected side chains are shown as sticks with red oxygens and blue nitrogens.

Fig. S7. Results of the MD simulations of the RUC-2–$\alpha_{IIb}\beta_3$ fragment complexes in the absence of the MIDAS Mg^{2+} ion. (**A**) Representative snapshot from MD simulations of the RUC-2 (+1 charge)-αIIbβ3 fragment complex. (**B**) Representative snapshot from MD simulations of the RUC-2 (+2 charge)-αIIbβ3 fragment complex. (**C**) Minimum distance between either oxygen of the Glu-220 side chain and the nitrogen of the terminal, neutral amine of RUC-2. (**D**) Minimum distance between either oxygen of the Glu-220 side chain and the nitrogen of the terminal, charged amine of RUC-2.

Fig. S1

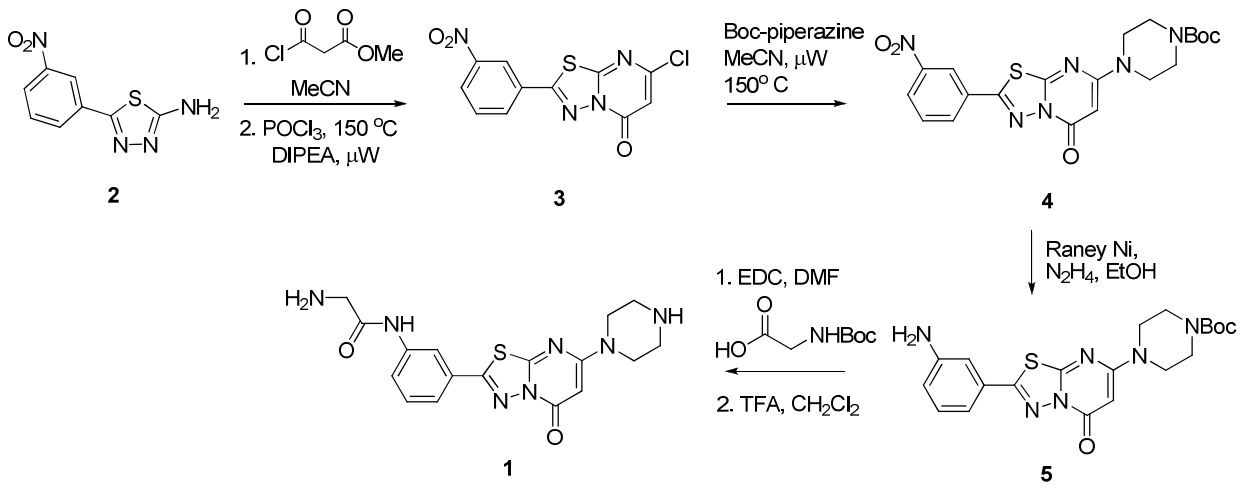

Abbreviations: MeCN, acetonitrile; $POCl_3$, phosphoryl chloride; DIPEA, *N*,*N*-diisopropylethylamine; μW, microwave; N_2H_4, cis-diazene; EtOH, ethyl alcohol; DMF, dimethyl formamide; TFA, tetrahydrofluoric acid; CH_2Cl_2, dichloromethane.

Fig. S2

A

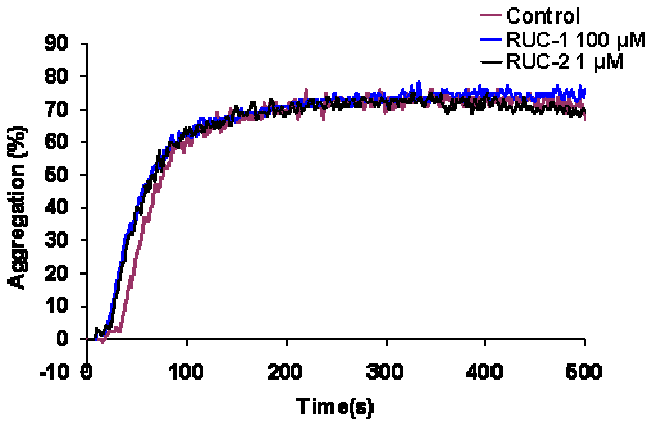
Control
RUC-1 100 μM
RUC-2 1 μM
Aggregation (%)
Time(s)

B

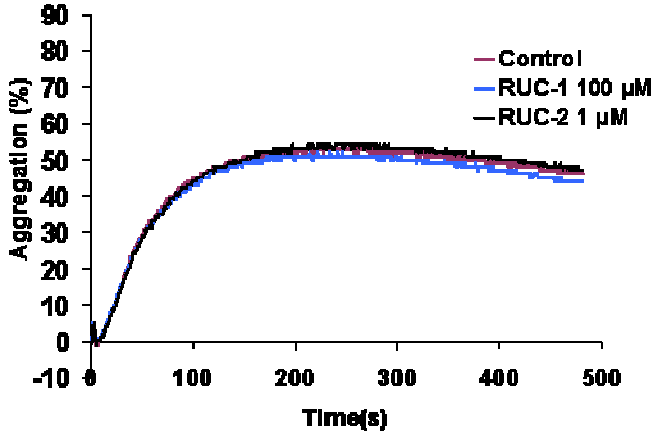
Control
RUC-1 100 μM
RUC-2 1 μM
Aggregation (%)
Time(s)

C

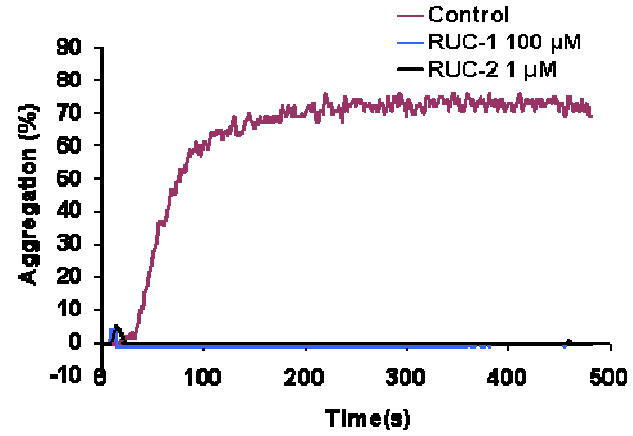
Control
RUC-1 100 μM
RUC-2 1 μM
Aggregation (%)
Time(s)

Fig. S3

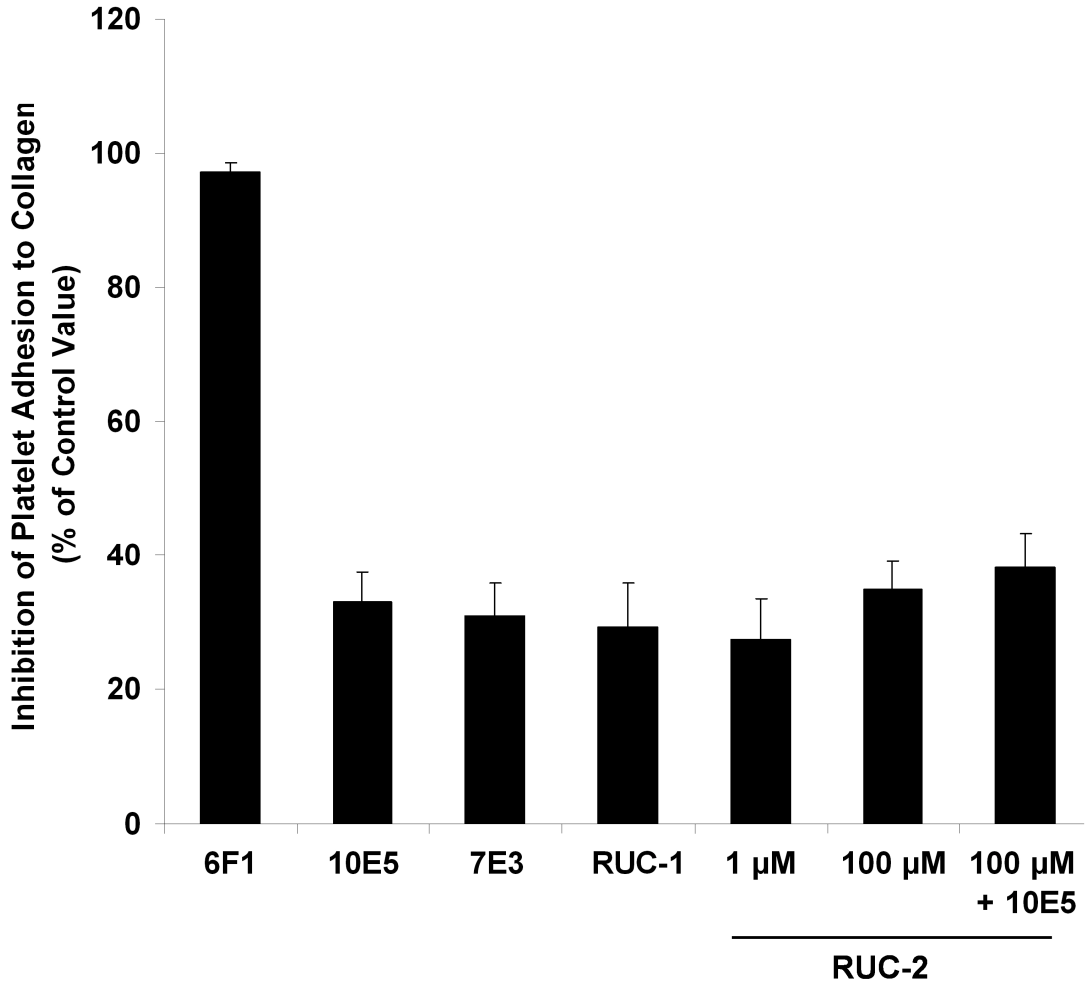
Inhibition of Platelet Adhesion to Collagen
(% of Control Value)
120
100
80
60
40
20
0
6F1
10E5
7E3
RUC-1
1 μM
100 μM
100 μM
+ 10E5
RUC-2

Fig. S4

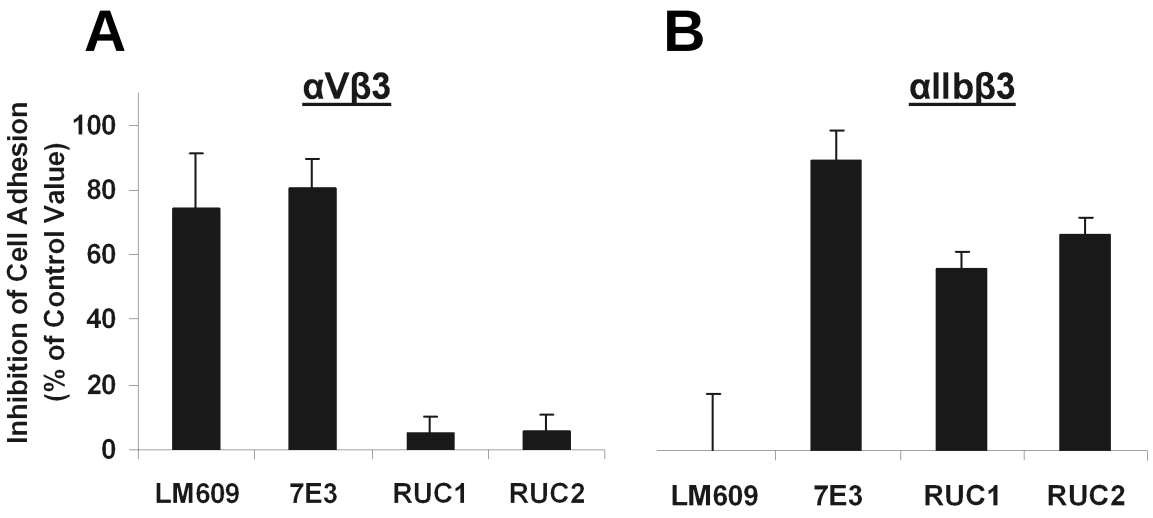
A
αVβ3
Inhibition of Cell Adhesion
(% of Control Value)
100
80
60
40
20
0
LM609
7E3
RUC1
RUC2
B
αIIbβ3
LM609
7E3
RUC1
RUC2

Fig. S5

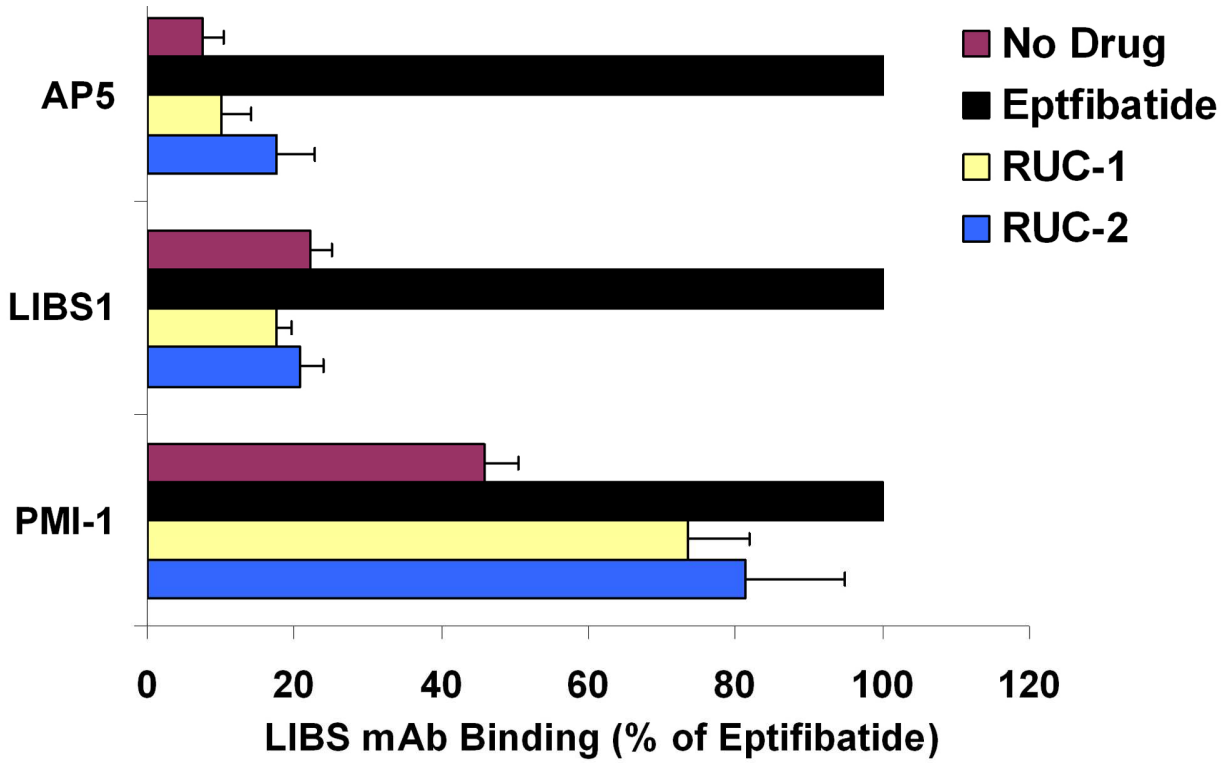
AP5
LIBS1
PMI-1
No Drug
Eptfibatide
RUC-1
RUC-2
0
20
40
60
80
100
120
LIBS mAb Binding (% of Eptifibatide)

Fig. S6

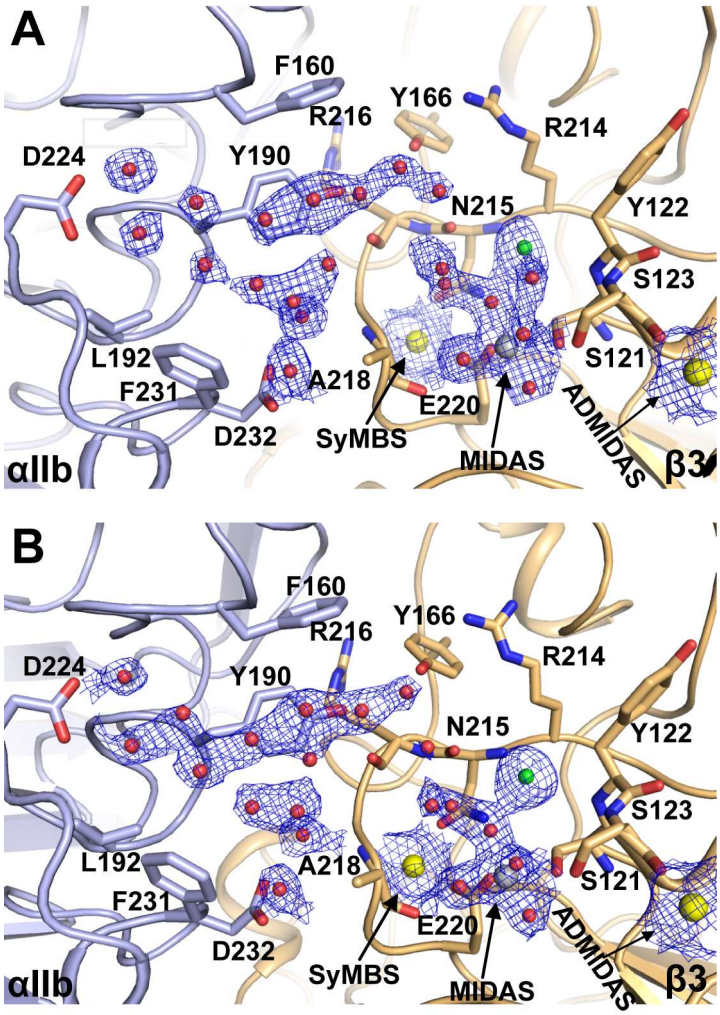
A
F160
R216
Y166
R214
D224
Y190
N215
Y122
S123
L192
F231
A218
E220
S121
D232
SyMBS
MIDAS
ADMIDAS
αIIb
β3
B
F160
R216
Y166
R214
D224
Y190
N215
Y122
S123
L192
F231
A218
E220
S121
D232
SyMBS
MIDAS
ADMIDAS
αIIb
β3

Fig. S7

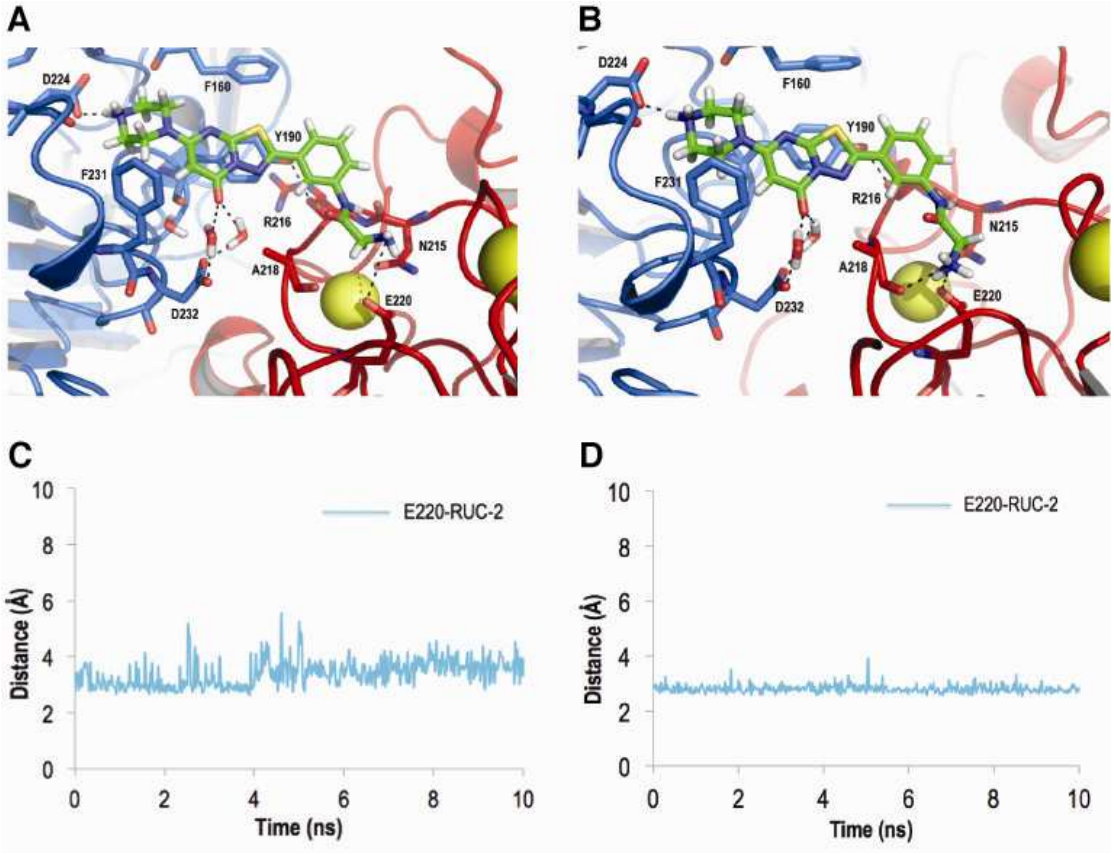
A
D224
F160
Y190
F231
R216
N215
A218
E220
D232
B
D224
F160
Y190
F231
R216
N215
A218
E220
D232
C
E220-RUC-2
Distance (Å)
Time (ns)
D
E220-RUC-2
Distance (Å)
Time (ns)

References

1. M. Tokuhira, M. Handa, T. Kamata, A. Oda, M. Katayama, Y. Tomiyama, M. Murata, Y. Kawai, K. Watanabe, Y. Ikeda, A novel regulatory epitope defined by a murine monoclonal antibody to the platelet GPIIb-IIIa complex ($\alpha_{IIb}\beta_3$ integrin). *Thromb. Haemost.* **76**, 1038–1046 (1996).
2. T. K. Ritchie, Y. V. Grinkova, T. H. Bayburt, I. G. Denisov, J. K. Zolnerciks, W. M. Atkins, S. G. Sligar, Reconstitution of membrane proteins in phospholipid bilayer nanodiscs. *Methods Enzymol.* **464**, 211–231 (2009).
3. T. H. Bayburt, S. G. Sligar, Membrane protein assembly into nanodiscs. *FEBS Lett.* **584**, 1721–1727 (2010).
4. F. Ye, G. Hu, D. Taylor, B. Ratnikov, A. A. Bobkov, M. A. McLean, S. G. Sligar, K. A. Taylor, M. H. Ginsburg, Recreation of the terminal events in physiological integrin activation. *J. Cell Biol.* **188**, 157–173 (2010).
5. R. Blue, M. Murcia, C. Karan, M. Jirouskova, B. S. Coller, Application of high-throughput screening to identify a novel αIIb-specific small-molecule inhibitor of αIIbβ3-mediated platelet interaction with fibrinogen. *Blood* **111**, 1248–1256 (2008).
6. J. Zhu, J. Zhu, A. Negri, D. Provasi, M. Filizola, B. S. Coller, T. A. Springer, Closed headpiece of integrin $\alpha_{IIb}\beta_3$ and its complex with an $\alpha_{IIb}\beta_3$-specific antagonist that does not induce opening. *Blood* **116**, 5050–5059 (2010).
7. R. Blue, M. A. Kowalska, J. Hirsch, M. Murcia, C. A. Janczak, A. Harrington, M. Jirouskova, J. Li, R. Fuentes, M. A. Thornton, M. Filizola, M. Poncz, B. S. Coller, Structural and therapeutic insights from the species specificity and in vivo antithrombotic activity of a novel αIIb-specific αIIbβ3 antagonist. *Blood* **114**, 195–201 (2009).
8. D. M. Lorber, B. K. Shoichet, Hierarchical docking of databases of multiple ligand conformations. *Curr. Top. Med. Chem.* **5**, 739–749 (2005).
9. E. C. Meng, B. K. Shoichet, I. D. Kuntz, Automated docking with grid-based energy evaluation. *J. Comp. Chem.* **13**, 505–524 (1992).
10. M. J. Frisch, G. W. Trucks, H. B. Schlegel, G. E. Scuseria, M. A. Robb, J. R. Cheeseman, J. A. Montgomery Jr., T. Vreven, K. N. Kudin, J. C. Burant, J. M. Millam, S. S. Iyengar, J. Tomasi, V. Barone, B. Mennucci, M. Cossi, G. Scalmani, N. Rega, G. A. Petersson, H. Nakatsuji, M. Hada, M. Ehara, K. Toyota, R. Fukuda, J. Hasegawa, M. Ishida, T. Nakajima, Y. Honda, O. Kitao, H. Nakai, M. Klene, X. Li, J. E. Knox, H. P. Hratchian, J. B. Cross, V. Bakken, C. Adamo, J. Jaramillo, R. Gomperts, R. E. Stratmann, O. Yazyev, A. J. Austin, R. Cammi, C. Pomelli, J. W. Ochterski, P. Y. Ayala, K. Morokuma, G. A. Voth, P. Salvador, J. J. Dannenberg, V. G. Zakrzewski, S. Dapprich, A. D. Daniels, M. C. Strain, O. Farkas, D. K. Malick, A. D. Rabuck, K. Raghavachari, J. B. Foresman, J. V. Ortiz, Q. Cui, A. G. Baboul, S. Clifford, J. Cioslowski, B. B. Stefanov, G. Liu, A. Liashenko, P. Piskorz, I. Komaromi, R. L. Martin, D. J. Fox, T. Keith, M. A. Al-Laham, C. Y. Peng, A. Nanayakkara, M. Challacombe, P. M. W. Gill, B. Johnson, W. Chen, M. W. Wong, C. Gonzalez, J. A. Pople, Gaussian 03, Revision C.02 (Gaussian, Inc., Wallingford, CT, 2004).
11. J. Wang, R. M. Wolf, J. W. Caldwell, P. A. Kollman, D. A. Case, Development and testing of a general amber force field. *J. Comput. Chem.* **25**, 1157–1174 (2004).
12. J. Aqvist, Ion-water interaction potentials derived from free energy perturbation simulations. *J. Phys. Chem.* **94**, 8021–8024 (1990).
13. T. A. Darden, D. York, L. G. Pedersen, Particle mesh Ewald: An *N*-log(*N*) method for Ewald sums in large systems. *J. Chemical Physics* **98**, 10089–10093 (1993).

14. J.-P. Ryckaert, G. Ciccoti, H. J. C. Berendsen, Numerical integration of the cartesian equations of motion of a system with constraints: Molecular dynamics of *n*-alkanes. *J. Computational Physics* **23**, 327–341 (1977).
15. D. W. Bougie, P. R. Wilker, E. D. Wuitschick, B. R. Curtis, M. Malik, S. Levine, R. N. Lind, J. Pereira, R. H. Aster, Acute thrombocytopenia after treatment with tirofiban or eptifibatide is associated with antibodies specific for ligand-occupied GPIIb/IIIa. *Blood* **100**, 2071–2076 (2002).